UNIVERSITY OF CALIFORNIA SAN DIEGO

Discovery of novel root specific maize dolabralexin defenses: an expanding family of antibiotics

A Thesis submitted in partial satisfaction of the requirements

for the degree Master of Science

in

Biology

by

Ahmed Khalil

Committee in charge:

Professor Eric Schmelz

Professor Alisa Huffaker

Professor Jose Pruneda-Paz

2020

The Thesis of Ahmed Khalil is approved, and it is acceptable in quality and form for publication on microfilm and electronically:

_____

_____

_____

Chair

University of California San Diego

2020

TABLE OF CONTENTS

LIST OF FIGURES

LIST OF TABLES

ACKNOWLEDGEMENTS

First and foremost, I thank my family for giving me the opportunity to pursue my education here in the US and continuing to support me to this day with everything they able are to offer. I would not have been able to achieve any of my goals without their unwavering support, patience and encouragement.

I thank my thesis advisor and mentor Dr. Eric A. Schmelz and show my utmost gratitude for everything he has done to support me since I've joined his lab in 2017 and till today. I am very thankful for this wonderful opportunity that he has presented me through all my undergraduate and graduate career at UCSD. Dr. Schmelz was the first person to both introduce me to and make me fall in love with research. His fiery and burning passion for his research is truly something that amazes me. Dr. Schmelz has been and will continue to be one of the most influential and important figures in my life. I will always remember and be full of gratitude for his continued unwavering support. Furthermore, I to give my utmost gratitude to Dr. Alisa Huffaker for all the efforts she has made to support since joining the Schmelz lab in the Fall of 2017. Dr. Huffaker is one of the kindest and most compassionate people I've ever met. I also would like to thank my committee member Dr. Jose Pruneda-Paz for his contributions to facilitating research in Muir and role in the completion of my thesis.

I would like to thank all members of both the Schmelz and Huffaker labs for all their wisdom, care, and patience that I often relied upon during my research. Special thanks to Yezhang Ding for always being there for me to clear any confusion, misunderstandings and for helping me with my projects over the past two and a half years at the Schmelz Lab. I would like to express my gratitude to my friend and lab partner Evan Saldivar for always being there for me and for his wonderful friendship. Evan is one of the most decent people I've met on this planet.

Without him I wouldn’t have had such a wonderful time in lab. He has always kept a helping hand extended for me whenever I needed any help at all in any situation where he was able to help. Although we were never per se on the same project, he always found ways to make life easier for me. I would like to thank Dr. Philipp Weckwerth for being such a wonderful person to be around since joining the lab in 2017. It has truly been a pleasure. I would like to thank Dr. Keini Dressano for all the help and support she has given me on a number of projects. I would also like to thank her for being one of the kindest people I’ve met in my life. I would like to thank Elly Poretsky for always being there to help me solve any and all problems I’ve had in performing data analysis. I would like to thank MengXi Wu for being a wonderful lab partner and for all the help she has offered me. MengXi was a wonderful lab partner and would always try to help make my life easier by helping in any way she can. Last but not in any way least, I would like to thank Aysha Alani, Calvin Harris, and Armin Dafdasharr for being wonderful undergraduate members of our lab. I would like to convey my gratitude for all the help they gave me in conducting a great number of experiments that I would have instead been doing all on my own. I truly appreciate their dedication and work ethic.

ABSTRACT OF THE THESIS

Discovery of novel root specific maize dolabralexin defenses:
an expanding family of antibiotics

by

Ahmed Khalil

Master of Science in Biology

University of California San Diego, 2020

Professor Eric Schmelz, Chair

As the world's largest annually harvested crop, optimization of maize (*Zea mays*) protective biochemical defenses that impede pest and pathogen attack will be essential to mitigate significant yield losses that could compromise our global food security. To better understand the diversity of pathogen elicited maize antibiotics, we leveraged a rapid sample preparation technique termed Vapour Phase Extraction (VPE) coupled with mass spectrometry (MS), high-performance liquid chromatography (HPLC) and Nuclear Magnetic Resonance

(NMR) spectroscopy. We focused experiments on roots of field-grown maize lines discovered to produce high levels of terpenoid defenses. Leveraging the power of VPE, HPLC, and NMR, we found a series of novel modified dolabradiene derivatives, predictably part of the dolabralexin diterpenoid family of maize defenses, termed 15,16-dinor-dolabradiol (DDD), Dolabranolic acid (DA), 16-nordolabranolic acid (NDA) and Dihydroxydolabrone (DHD). To generate endogenous evidence that the novel dolabralexins are products of diterpene synthases Anther ear 2 (ZmAn2) and Kaurene Synthase-Like 4 (ZmKSL4), we analyzed *Zman2* and *Zmksl4* mutants and demonstrated an absence of all dolabralexin-related metabolites. Chemical analyses of maize Biparental Recombinant Inbred Line (RIL) mapping population and an association panel coupled with global gene co-expression analyses using Mutual Ranks and Agrobacterium-mediated transient overexpression enzyme assays in *Nicotiana benthamiana* using different combinations of ZmAn2 and ZmKSL4 with cytochrome (CYP) P450 monooxygenases have revealed that ZmCYP71Z16 may contribute to the production of complex dolabralexin products.

Introduction

To combat complex biotic stresses such as insect and pathogen attack, all plants rely on small-molecule specialized metabolites to serve as direct and indirect defenses (Dixon 2000 Rev). Present in all plants terpenoids are the most structurally diverse class of specialized metabolites known among plant biosynthetic pathways. Unlike classical models such as conifers, maize only recently has been recognized to rely on diverse volatile terpenoid precursors for the production of microbially elicited non-volatile antibiotics. Despite being a predominant global crop and research model, comprehensive examinations of maize tissues challenged with microbes continue to reveal additional and previously hidden terpenoids of biological significance. Terpenoids display massive structural diversity with over 25,000 known compounds. Additionally, they have many different roles which include phytohormones, serving as chemical barriers, and mediating interactions between the plant and other surrounding organisms (Gershenzon and Dudareva, 2007). Following insect attack, certain maize volatile terpenes serve as defense metabolites in both the roots and shoots (Turlings *et al*., 1990; Degenhardt, 2009; Degenhardt *et al*., 2009a; Köllner *et al*., 2013). In maize, isoprenoid precursors also serve as building blocks for modified non-volatile antibiotic terpenoid defenses (Schmelz *et al*., 2014). Although commonly undetectable as volatile precursors, the elicited accumulation of non-volatile terpenoids can limit plant damage caused by pathogens, oxidative stress, and herbivory. (Harborne, 1999; Ahuja *et al*., 2012) (Ding et al., 2019 Nat Plant; and https://doi.org/10.1101/2020.03.04.977355). Despite advances, research in maize continually demonstrates that our knowledge of biochemical defenses and pathway genes responsible for mitigating stresses on crops remains incomplete.

Terpenes and mono-oxygenated terpenoids are common components of maize volatiles following biotic stress (Turlings et al. 1990; Ding et al. 2017). Thus, a more comprehensive examination of novel semi-volatile and non-volatile metabolites are predicted to reveal specialized metabolites of biological relevance. As a biosynthetic family, the largest known example in maize are the non-volatile acidic sesquiterpenoids termed zealexins produced in response to attack by diverse fungal species. The zealexin (Zx) family consists of least 17 precursors and products derived from a Chromosome 10 gene cluster of 4 Terpene Synthases (TPS), now termed *Zx1* through *Zx4*, that encode β-bisabolene dependent β-macrocarpene synthases that are functionally variable across inbreds (Huffaker *et al.*, 2011; Ding *et al.*, 2020). A second zealexin pathway gene cluster on Chromosome 5 contains three promiscuous CYP71Z family cytochrome P450 genes; termed *Zx5* (*ZmCYP71Z19*), *Zx6* (*ZmCYP71Z18*) and *Zx7* (*ZmCYP71Z16*). Zx5, Zx6 and Zx7 collectively catalyze oxidation of β-bisabolene and β-macrocarpene to form D-series and A-series zealexins (ZA1). Zx5 has additionally been shown to act on α/β-selinene producing α/β-costic acids; a α/β-selinene derived sesquiterpenoids (Ding *et al.*, 2020). Similarly, Zx6 and Zx7 share in catalyzing several oxidative steps in both the dolabralexin and kauralexin diterpenoid defense pathways (Mafu et al., 2018; Ding et al., 2019). Zealexin complexity is further expanded by a gene cluster of 3 CYP81A family P450s on Chromosome 1, termed *Zx8*, *Zx9* and *Zx10*, that encode enzymes involved in oxygenation and desaturation reactions. The majority of the zealexin structural diversity is derived from Zx8, Zx9 and Zx10 action on the ZA1 substrate. It has been shown that *zx1 zx2 zx3 zx4* quadruple mutants are blocked in the pathogen elicited production of β-bisabolene & β-macrocarpene and all known zealexins resulting in a broad-spectrum loss of disease resistance (Ding *et al.*, 2020).

Beyond sesquiterpenoids, diterpenoid derived antibiotics are components of diverse biochemical defenses in maize (Schmelz et al., 2011; Mafu et al.,2018; Ding et al. 2019). Following fungal elicitation, maize produces *ent*-copalyl pyrophosphate synthase (*ent*-CPS) derived diterpenoids, termed kauralexins and dolabralexins, derived from *ent*-isokaurene and dolabradiene, respectively. The sequential activity of the maize *ent*-CPS, termed Anther Ear 2 (ZmAn2 or An2), and Kaurene Synthase-Like 2 (ZmKSL2 or KSL2) is required for the biosynthesis of the kauralexin pathway precursor *ent*-isokaurene (Ding *et al*., 2019). Oxygenation and subsequent desaturation of *ent*-isokaurene by three promiscuous cytochrome P450s and a steroid 5α-reductase namely, kaurene oxidase 2 (ZmKO2 [KO2], ZmCYP701A43), ZmCYP71Z16/18 and kauralexin reductase 2 (ZmKR2 or KR2, Zm00001d018847), indirectly yields the predominant *ent*-kaurene-associated antibiotic, namely kauralexin A3, required for *Fusarium* stalk rot resistance (Ding *et al*., 2019).

An additional diterpenoid biosynthetic pathway branch that emerges from ZmAn2 derived *ent*-CPP is the dolabralexin pathway (Mafu et al., 2018). Dolabralexin biosynthesis involves the sequential activity of the type II diterpene synthase ZmAn2 and the type I diterpene synthase Kaurene Synthase-Like 4 (ZmKSL4 or KSL4). Together, ZmAn2 and ZmKSL4 form the diterpene hydrocarbon dolabradiene. Subsequently, the oxidation of dolabradiene by the partially redundant cytochrome P450 monooxygenases, ZmCYP71Z18 and ZmCYP71Z16, yield the epoxides 15,16-epoxydolabrene (epoxydolabrene) and 3β-hydroxy-15,16-epoxydolabrene (epoxydolabranol) (Mafu *et al*. 2018). The absence of dolabradiene and epoxydolabranol in *Zman2* (*an2*) mutants under elicited conditions confirmed the *in vivo* biosynthetic requirement of ZmAn2. Additionally, epoxydolabranol is further converted into 3β,15,16-trihydroxydolabrene (trihydroxydolabrene) which was found to exist the dominant end product

accumulating in elicited root tissues (Mafu *et al*. 2018). Dolabralexin biosynthesis is widespread across all examined maize cultivars. Oxidative stress induces dolabralexin accumulation and variable transcript expression of *ZmAn2* and *ZmKSL4* in root tissues. Furthermore, metabolite and transcript accumulation are partly up-regulated in response to elicitation with the fungal pathogens *Fusarium verticillioides* (*F.v.*) and *Fusarium graminearum* (*F.g.*) (Mafu *et al*. 2018). Consistently, low doses of epoxydolabranol in the range of 10 to 50 μg ml^{-1} significantly inhibited the growth of *F.v.* and *F.g. in vitro*. Trihydroxydolabrene-mediated fungal growth inhibition was specific to *F.v.*. Thus dolabralexins appear to have defense-related roles in maize biotic stress protection and represent the newest maize family expanded diterpenoid defenses (Mafu *et al*. 2018). Additionally, loss of both kauralexin and dolabralexins in *Zman2* mutants (Christensen et al., 2018) and specifically kauralexins *Zmksl2* mutants (Ding *et al.*, 2019) have been shown to cause increased fungal susceptibility.

Given the recent discovery of dolabralexins in maize a number of outstanding questions remain. For example, ZmKSL2 is ultimately responsible for at least 2 hydrocarbon olefins and 8 accumulated kauralexin family end products. Might there be an even larger family of root specific dolabralexins than previously reported in Mafu et al. (2018)? Why have dolabralexins gone unnoticed for so long by other researchers? How can dolabralexins be easily and routinely detected to facilitate research into demonstrating biological roles in the field? Trihydroxydolabrene accumulation in fungal-elicited root tissues appears to be a less effective antifungal agent that the required pathway precursors. Might other as yet unknown derivatives of epoxydolabranol and trihydroxydolabrene serve useful antibiotic functions?

The goal of this effort was to identify additional novel defense metabolites and their corresponding synthetic pathways to better understand the biochemical basis of maize innate

immunity. The production and regulation of defensive specialized metabolites play a central role in pathogen resistance in all plants (Dixon 2001, review). Ultimately the understanding and long-term optimization of protective plant specialized metabolites that serve to impede pest and pathogen attack will be essential tools in the targeted management in stress related yield losses.

Materials and Methods

Biological materials used

Maize plants were grown in the greenhouses and fields at the UCSD Biology Field Station (BFS). Goodman association panel seeds were obtained from the National Genetic Resources Program (GRIN; https://www.ars-grin.gov/) spanning 294 inbred lines. Biparental, PHW65xMoG (PM), mapping population seeds, were a kind gift from Dr. Natalia de Leon (Department of Agronomy, University of Wisconsin) (Gage et al., 2018). For forward genetic studies, maize plants typically 40 days old grown in the BFS field and exposed to naturally occurring pathogens. Plant were dug from the soil, root systems were washed with H_2O, frozen with liquid N_2, ground in liquid N_2 to a fine powder and stored at −80°C. Working with liquid N_2 and −80°C is essential to halt all enzyme activities and maintain stability of potentially labile analytes.

Chemical Analyses using Gas Chromatography/Mass Spectrometry (GC/MS)

A simple approach to sample analysis relies on Vapor Phase Extraction (VPE) to remove high molecular weight analytes otherwise un-compatible with gas chromatography (GC). In this

procedure typically 50 mg sample aliquots are weighed, extracted by organic solvent during vortexing/bead homogenization and the resulting organic phase is derivatized using trimethylsilyl diazomethane (Schmelz *et al*., 2004). VPE for a select number of samples were performed following Schmelz *et al*., (2004) using an Agilent 6890 series GC coupled to an Agilent 5973 mass selective detector (MSD) is described further below. Agilent Mass Hunter Qualitative and MS Quantitative Analysis software alongside Agilent ChemStation qualitative programs were used to generate and analyze the GC-MS generated chromatograms and spectra. Replicated experiments were summarized with peak areas captured in MassHunter Qualitative Navigator B.08.00, and MS Quantitative Analysis B.08.00, quantified in Excel and statistically evaluated in JMP. MassHunter MS Quantitative program peak selection methods were manually produced taking into account retention time shifts. Program automated peak selections/integrations were instead substituted for manual selections/integrations of every target compound in every sample. This allowed for a much greater degree of accuracy in calculating compound concentrations and better overall genetic mapping.

A Modified and Improved Vapor Phase Extraction (VPE) Protocol

To minimize artifact generation, biologic samples were frozen in liquid N_2 and maintained at -80°C immediately prior to solvent extraction. Root and leaf tissue samples were pulverized a fine powder in liquid N_2 to generate homogenous aliquots. Special notice: In a previously published VPE protocol (Schmelz et al., 2004) the method made extensive use of tissue extraction using plastic tubes and bead mill homogenizer. In the current modification, a tissue homogenizer is avoided due to aggressive sample and solvent contact with plastic. This change necessitates extra care in sample grinding to ensure a fine powder is generated enabling

efficient extraction via the simple contact with solvent alone. Tissue (50-60 mg) was placed into a 4 ml glass vial kept on liquid N_2. Special notice: For the routine analysis of diverse oxygenated plant terpenoids ALL handling steps including solvent pipetting, liquid handling, storage, and transfers requires glass syringes and glass vials. If at any point solvents contact plastics in the sample preparation process, the sample will be contaminated and result in potentially permanent poor chromatography preventing detection of predominant analytes. This aspect cannot be emphasized enough. The only step where plastics do not pose a problem is in the storage of -80C pulverized tissue samples prior to extraction. All other steps must avoid all contact at any step with plastics. Teflon liners on solvents are helpful and do not harm samples. Polyethylene liners ("cone caps") on 20 ml sample vials appear to be useable with caution, ideally liquid solvents do not come into direct physical contact with the lid. Immediately prior to extraction, finely ground samples in 4 ml glass vials are removed from the liquid N_2 and spiked with 500 µls of the extraction solvent, namely H_2O: 1-propanol: HCl (1:2:0.005) with internal standards (described in Schmelz *et al*., 2004). This is accomplished using an adjustable Eppendorf 1ml pipettor modified with a Tygon adaptor to grip a 5-3/4" inch glass pipette tip enabling clean solvent transfers. A Teflon lined cap is then screwed on the vial and the sample is vortexed for 1 min and allowed to sit for 5 min. Next 1 ml of hexane is further added using a glass pipette tip, the vial is re-capped, briefly re-vortexed and allowed to settle for 10 min. The lower aqueous and upper hexane:1-propanol layers concentrate highly polar and lipophilic metabolites, respectively. Use of internal standards quantitatively corrects for potential pH-derived differences in extraction efficiency between samples.

To increase volatility and improve gas phase chromatography of carboxylic acid containing analytes, the upper organic phase is transferred to a new clean 4-ml glass vial and

derivatized directly using 7 μl of trimethylsilyldiazomethane (2M in hexane)(Sigma-Aldrich) to generate to methyl esters following gentle shaking and a 15 min reaction time. A dedicated 10 ul volumetric glass syringe (Agilent) is used for trimethylsilyldiazomethane transfer. Unlike previous VPE protocols (Schmelz et al., 2004) excess trimethylsilyldiazomethane is not neutralized with excess acetic acid. Instead, in a fume hood, excess solvents and trimethylsilyldiazomethane are removed under a N_2 stream to dryness. For analyses seeking to include volatile analytes, such as sesquiterpene and diterpene hydrocarbon olefins, the user must only go past dry for a few seconds as any further drying will remove analytes of interest. Special notice: If the derivatized analytical sample is either is neutralized while in liquid or not taken to dryness prior to VPE, the sample will contain unacceptable levels of reacted and unreacted trimethylsilyldiazomethane products that damage the GC column and prevent polar metabolite analyses. This is the second misstep whereby the detection of oxygenated terpenoids can be severely impaired. Any sample not properly processed requires starting over with a new 50 aliquot. Semi-volatile trimethylsilyldiazomethane derived contaminants cannot be removed by further rounds of attempted VPE clean up steps.

The volatile collection filters, termed VPE traps, are constructed from inert materials including glass, fluorocarbons, and stainless-steel/nylon mesh. Special notice: With handling care VPE traps can be re-used almost indefinitely. Care of VPE traps includes a series of solvent washes for cleaning immediately prior to each use. The suggested solvent series is the serial application of 500 μl aliquots of ultra-pure H_2O (LCMS grade), followed by 1-propanol and finally ethyl acetate. Other clean solvents can be used as well but they should be a range of co-miscible solvents that span a range of polarities and have sufficient eluting strength spanning both polar to non-polar compounds. The adsorbent present in VPE traps is Porapak Q (80-100

μm mesh termed Super Q) (Sigma Aldrich), a divinylbenzene polymer tolerant most solvents and sensitive only to temperatures above 300°C or the presence of strong oxidizing acids. To make use of Porapak Q properties and increase the range of analytes recovered, volatilization temperatures of 200°C were used (Schmelz *et al*., 2004). A N_2 stream is used to reduce sample oxidation. Working in the fume hood, the collection of VPE samples requires approximately 2 mins. Sample collection procedure is as follows: (i) N_2 stream through the needle is initiated with surplus pressure released to a bubbler with the existing flow exceeding the vacuum once the system is fully linked. (ii) A 500 ml min^{-1} flow is generated by chemically resistant teflon-membrane vacuum pump calibrated with a needle valve and periodically confirmed using a flowmeter. (iii) The VPE trap is first inserted into the high temperature septa, followed by the N_2 stream needle, and finally the Teflon vacuum line is connected to the VPE trap. Upon proper connection, solvent vapors pass through the VPE trap and the collection of volatile analytes is initiated. At this time, the dry vial is transferred to a heating block at 200°C for 2 min. Once the VPE collection process is completed, the sample is disassembled by handling the vacuum and N_2 supply lines and open top caps, with care taken to avoid touching the heated glass. For analysis, the VPE trap are eluted into a GC/MS sample vial with 200 μls of ethyl acetate: hexane (1:1) transferred using a chemically inert syringe (glass and Teflon) and analyzed by GC/MS.

Specifically for tobacco (*Nicotiana benthamiana*) metabolite analyses, prior to the extraction described above, tissue aliquots were subjected to β-glucosidase treatment (Sigma-Aldrich, Co, LLC, USA) in 250 μl 0.1 M sodium acetate buffer (pH=5.5) at a concentration of 100 units ml^{-1} at 37°C for 30 minutes before solvent extraction.

Gas chromatography/mass spectrometry (GC/MS) analyses of metabolites

GC/MS analysis were made using an Agilent 6890 series gas chromatograph joined to an Agilent 5973 mass selective detector (mass temperature,150 °C; interface temperature, 250 °C; electron energy, 70 eV; source temperature, 230°C). DB-35 MS column (Agilent; 30 m × 250 μm × 0.25 μm film) was used for gas chromatography. Samples were introduced, with an initial oven temperature of 45 °C, as a splitless injection. The temperature was held for 2.25 min, then increased to 300 °C with a gradient of 20 °C min^{-1} and held at 300 °C for 5 min. A solvent delay of 4.5 min was selected to prevent ethyl acetate present in the sample from damaging the EI-filament. GC–MS-based quantification of dolabralexins utilized external standard curve of 15,16-dinor-dolabradiol (DDD) and the predominant fragment ion 193 *m*/*z* typically eluting at 16.4 min. 15,16-dinor-dolabradiol was discovered over the course of this work. Standard GC–MS analysis of maize metabolites and *N. benthamiana-in vivo* expressed enzyme products was performed on the same instrument. Product identification of previously known analytes was conducted using authentic standards and where possible by comparing reference mass spectra with Wiley, National Institute of Standards and Technology and the Adams libraries.

***Transient enzyme co-expression assays in tobacco* (*N. benthamiana*)**

For transient expression in *N. benthamiana*, pLIFE33 constructs carrying individual target genes and pEarleyGate100 with *El*HMGR159–582 construct were electroporated into Agrobacterium tumefaciens strain GV3101. To ensure detectable production of sesquiterpenoid pathway products, all assays utilized co-expression of the coding sequence for truncated cytosolic *Euphorbia lathyris* 3-hydroxy-3-methylglutaryl-coenzyme A reductase (HMGR;

ElHMGR159–582, JQ694150.1) (Sadre *et al*., 2019). An *Agrobacterium tumefaciens* strain encoding the P19 protein was also equally added in order to suppress host gene silencing. *Agrobacterium* cultures were separately prepared at OD600 of 0.8 in 10 mM MES pH 5.6, 10 mM MgCl2, mixed together in equal proportion, and then infiltrated into the newly fully expanded leaves of six-week-old *N. benthamiana* plants using a needleless syringe. Five days post infiltration (dpi), *Agrobacterium*-inoculated tobacco leaves were collected, ground to a fine powder in liquid N_2 and stored at -80°C. Samples were then processed for metabolite analysis as described previously.

Purification, analyses and NMR of Novel Dolabralexins

For the purification of (2R,4βS,7S,10aR)-4b,7,10a-trimethyl-1-methylenetetradecahydrophenanthrene-2,7-diol (15,16-dinor-dolabradiol, DDD), 2-((2S,4aS,7R,8aR)-7-hydroxy-2,4a,8a-trimethyl-8-methylenetetradecahydrophenanthren-2-yl)acetic acid (dolabranolic acid, DA), (2S,4aS,7R,8aR)-7-hydroxy-2,4a,8a-trimethyl-8-methylenetetradecahydrophenanthrene-2-carboxylic acid (16-nordolabranolic acid, NDA), 2-hydroxy-1-((2S,4aS,7R,8aR)-7-hydroxy-2,4a,8a-trimethyl-8-methylenetetradecahydrophenanthren-2-yl)ethan-1-one (dihydroxydolabrone, DHD) and a dihydroxylated β-selinene-derivative identical to kudtdiol (CAS: 70142-90-4), 300 grams of 35-day-post-pollination field-grown MoG root tissue was ground to a fine powder in liquid N_2, extracted first with 500 mL of methanol then secondarily extracted with 500 mL of ethyl acetate (EA), filtered and dried using a rotary evaporator. The resulting oily residue was then allowed to partition and re-dissolve in 300 ml EA. The EA fraction was then dried down and the resulting

oily residue was then separated by preparative flash chromatography (CombiFlashRf; Teledyne ISCO) on a 5g C18, reverse phase, (RediSepRf High Performance GOLD) column. The mobile phase consisted of solvent A (100% H_2O) and solvent B (100% Acetonitrile), with a continuous gradient of 0-100% B from 1 to 81 min using a flow rate of 18 ml min^{-1}. 100 µl aliquots of these fractions were then derivatized using trimethylsilyldiazomethane, dried resolubilized in 200 µl of 1:1 hexane: ethyl acetate and analyzed by GC/MS. One fraction spanning 33-38 minutes contained an enrichment of the putative candidates for 15,16-dinor-dolabradiol (DDD). Likewise fractions at 39-42 min contained 16-nordolabranolic acid and dihydroxydolabrone, while dolabranolic acid and kudtdiol were found in fractions 43-46 min. Select concentrated samples were further purified by high performance liquid chromatography HPLC using repeated methylated/derivatized (using trimethylsilyldiazomethane) 1 mg injections (passed through silica to filter out precipitate following derivatization) on a Zorbax RX-silica (250 x 4.6 mm, 5 µm; Agilent) column and a mobile phase consisting of solvent A (100% Hexanes) and solvent B (100% EA) with a continuous gradient of A–B from 2 to 37 min using a flow rate of 1 ml min^{-1}. The recollected HPLC fractions spanning 13-14 min retention times (RT) yielded 16-nordolabranolic acid at ~90% purity, 16-17 min RT had the dihydroxydolabrone at ~95% purity, 21-22 min had kudtdiol at 95% purity, 14-15 min RT contained 15,16-dinor-dolabradiol at 95% purity, and 12-13 min had the C20-Acid at 90% purity were all used to generate samples for NMR. NDA and DA were isolated as methyl esters (NDA-ME, DA-ME). NDA-ME isolation posed a great challenge as it elutes 5-10 seconds prior to zealexin A5 methyl ester (ZA5-ME) elution (Ding *et al*., 2020). Repeated efforts were made to separate NDA-ME and ZA5-ME with only a few successful attempts. Due to the COVID19 situation we were not able to switch to a C18, reverse phase, acetonitrile-water purification for subsequent antifungal activity bioassays.

Purified DDD, DHD, DA-ME, NDA-ME and kudtdiol were dissolved in d_3-chloroform, and NMR spectra were acquired on 1D and 2D NMR spectra were measured on a Varian VX (500 MHz) spectrometer, equipped with a 5 mm $^{1}H\{^{13}C\}$ room temperature probe optimized for direct ^{13}C NMR measurements or a Bruker Avance III (600 MHz) NMR spectrometer with a 1.7 mm $^{1}H\{^{13}C/^{15}N\}$ microcryoprobe at room temperature and iNMR software. (More details on NMR spectroscopy methods and analysis are available through contacting the UCSD Molinski Lab; Dr. Tadeusz Molinski, tmolinski@ucsd.edu)

Source of Zman2, Zmksl2, and Zmksl4 Genetic Mutants

In support of the endogenous role of *ZmAn2*, a transposon insertion resulting in an *ZmAn2* null mutation utilized as described in Vaughan et al. (2015). *Zmksl2 and Zmksl4* genetic mutants were created using CRISPR–Cas9 was as outlined in Ding et al. (2019). The *Zmksl4* mutants were a kind gift of Zerbe laboratory (UC Davis).

In Vitro Antifungal Assays with 15,16-dinor-dolabradiol

As described previously maize antifungal assays using the Clinical and Laboratory Standards Institute M38-A2 guidelines were performed for 15,16-dinor-dolabradiol (Schmelz et al., 2011). Using a Synergy4 (BioTech Instruments) reader with a 96-well microtiter plate-based method through periodic measurements of changes in OD600, fungal growth at 30°C in broth medium was briefly monitored. 200 μL of primary fungal inoculum (2.5 3 10^4 conidia μL^{-1}) with 0.5 μL of either pure DMSO or DMSO containing dilutions of HPLC-purified root-derived 15,16-dinor-dolabradiol were in each well.

Analyses of global gene co-expression using Mutual Ranks

Basic calculations of co-expression summarized as Mutual Ranks were performed as described in Wisecaver *et al*. (2017). Given the vast number of calculations required and from a more practical standpoint, I worked with the Huffaker laboratory and specifically, PhD candidate Elly Poretsky and made use of an expanding RStudio Graphical User Interface program under development termed MutRank (version 0.9). As an end-user of this program, I used the Kremling *et al*. (2018) produced multi-tissue gene expression resource that represents the genotypic and phenotypic diversity of modern inbred maize, and includes 1960 transcriptomes spanning 300 inbred lines in seven tissues to produce the Mutual Rank scores.

Forward genetic mapping to uncover gene candidates influencing Dolabralexin production

To consider genetic variation in biparental mapping lines, we screened the biparental, PHW65 x MoG, mapping population (Gage *et al*., 2018). Additionally, to utilize genetic diversity in a larger population, we screened the Goodman diversity panel (Flint-Garcia *et al.* 2005). Association analyses were conducted in TASSEL 5.2.61 using the General Linear Model (GLM). Genotypic data from imputed PHW65 x MoG SNP markers were used to generate ~150,000 SNP markers (. GWAS analyses utilized the B73 version 3 referenced HapMap consisting of 246,477 SNPs as described (Samayoa et al. 2015). Manhattan plots were constructed in TASSEL and RStudio.

Results

Discovery of Novel Dolabralexins

To better understand the diversity of pathogen elicited maize antibiotics, we leveraged and highly modified a rapid sample preparation technique termed Vapour Phase Extraction (VPE) (Schmelz *et al.*, 2004) covered in detail in the current Materials and Methods section. We sought to increase the number of metabolites that we are able to routinely detect in our analyses to further elucidate biochemicals and enzymes that constitute integral maize defense pathways. VPE is a robust method which enables the detection of a large array of hydrophobic and amphipathic small molecules. In 2019, we began a series of successful trials in an effort to improve our reproducible gas chromatography of increasingly oxygenated (mainly hydroxylated) terpenoids such as zealexin A3 and zealexin B3. The main advance was removing all traces of the trimethylsilyldiazomethane derivatization agent prior to VPE sample collection and doing all manipulations in a plastic free workflow. The purification of metabolites not previously detected in necrotic maize tissues was then initiated. Trials were performed on roots of field grown MoG; a maize line we discovered to reproducibly produce high levels of terpenoid defenses (Figure 1. B). Following extraction with methanol and ethyl acetate and initial clean-up using C18 flash chromatography, we leveraged normal phase (silica) HPLC to purify novel terpenoids from MoG root tissue extracts rich in sesquiterpenoids. Nuclear Magnetic Resonance (NMR) spectroscopy based structural elucidation revealed a novel modified 18 carbon dihydroxylated dolabradiene derivative (Fig 1A), termed 15,16-dinor-dolabradiol **(**DDD), predictably part of the dolabralexin diterpenoid family of maize defenses (Mafu et al. 2018). The parent ion of 278 *m*/*z* of this dominant root metabolite was unexpected for a diterpenoid and matched that of highly oxygenated sesquiterpenoids, such as zealexin A9 methyl ester (Ding 2020, Nature Plants paper). Mindful that novel and previously unknown dolabralexin derivatives existed in roots, we pursued a series of related HPLC based purifications and NMR analyses resulting in additional

dolabradiene-derived novel defenses, termed dihydroxydolabrone (DHD), dolabranolic acid, DA), 16-nordolabranolic acid (NDA) (Figure 1. A, B). Using an iterative approach, we also isolated and identified a dihydroxylated β-selinene-derivative identical to kudtdiol (CAS: 70142-90-4) that similarly requires a functional copy of *ZmTPS21* the maize β-selinene synthase (Figure 1. A, B, C) (Ding *et al*. 2017).

Figure 1, Continued. Newly Discovered Maize Dolabradiene-Derived Diterpenoids Part of the Dolabralexin Defense Pathway. A, Field collected MoG root tissues were utilized for HPLC based purification followed by NMR spectroscopy analysis (in collaboration with the UCSD Molinski Lab) resulted in the following four novel dolabradiene derived chemical

structures; DDD, DHD, DA, NDA and kudtdiol. B, GC/MS Total ion chromatogram (TIC) of vapour phase extracted microbially-elicited MoG root tissues used in novel dolabralexin purification protocols. Compounds 1-8, labeled above, were identified base on retention time (RT) and mass spectrum comparison. Compound 1 is β-costic acid, 2 is kudtdiol, 3 is DDD, 4 is NDA-ME, 5 is an uncharacterized diterpenoid, 6 is DHD, 7 is DA-ME and 8 is an uncharacterized diterpenoid. C-G, panels top to bottom, are GC/MS extracted ion chromatograms EIC of kudtdiol (compound 2), DDD (compound 3), NDA-ME (compound 4), DHD (compound 6), and DA-ME (compound 7), respectively. H-L, panels top to bottom, are GC/MS EI mass spectra of kudtdiol (compound 2), DDD (compound 3), NDA-ME (compound 4), DHD (compound 6), and DA-ME (compound 7), respectively.

(A)

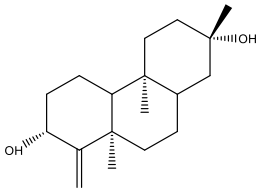

15,16-dinor-dolabradiol (DDD)(Compound 3)

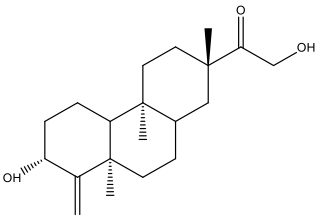

Dihydroxydolabrone (DHD)(Compound 6)

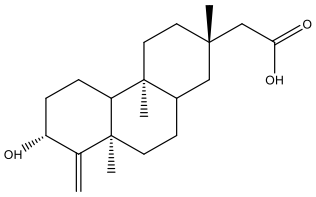

Dolabranolic acid (DA)(Compound 7)

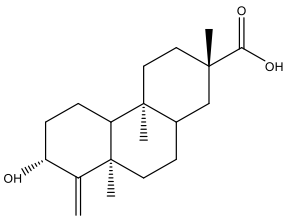

16-nordolabranolic acid (NDA)(Compound 4)

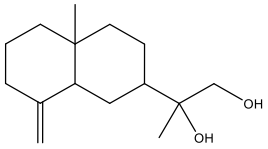

Kudtdiol (Compound 2)

(B)

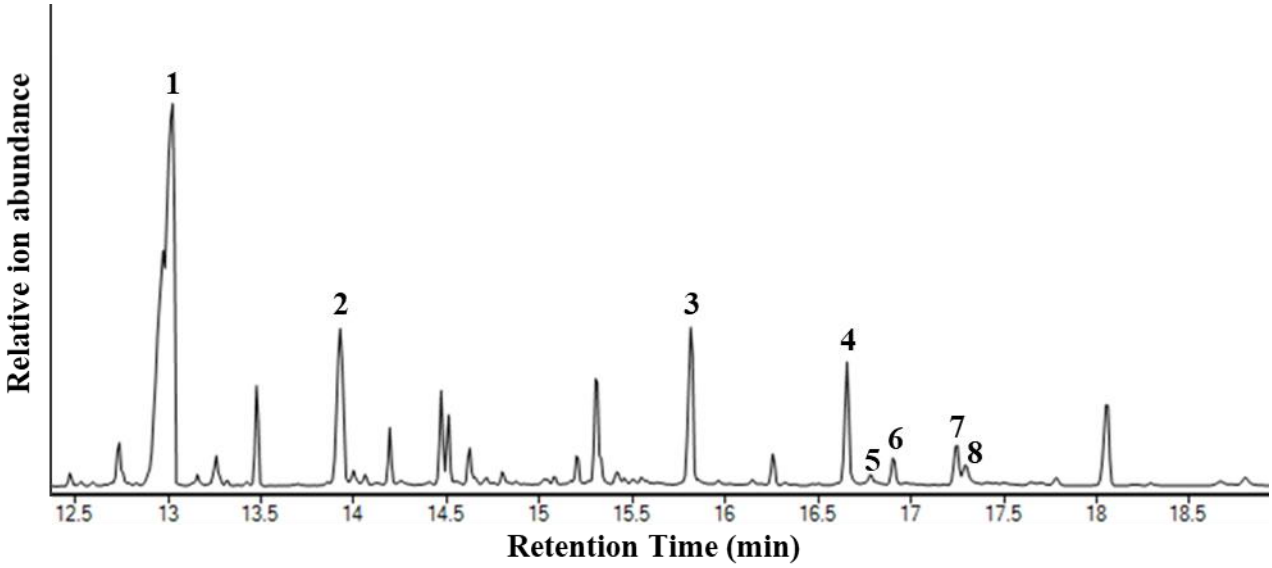

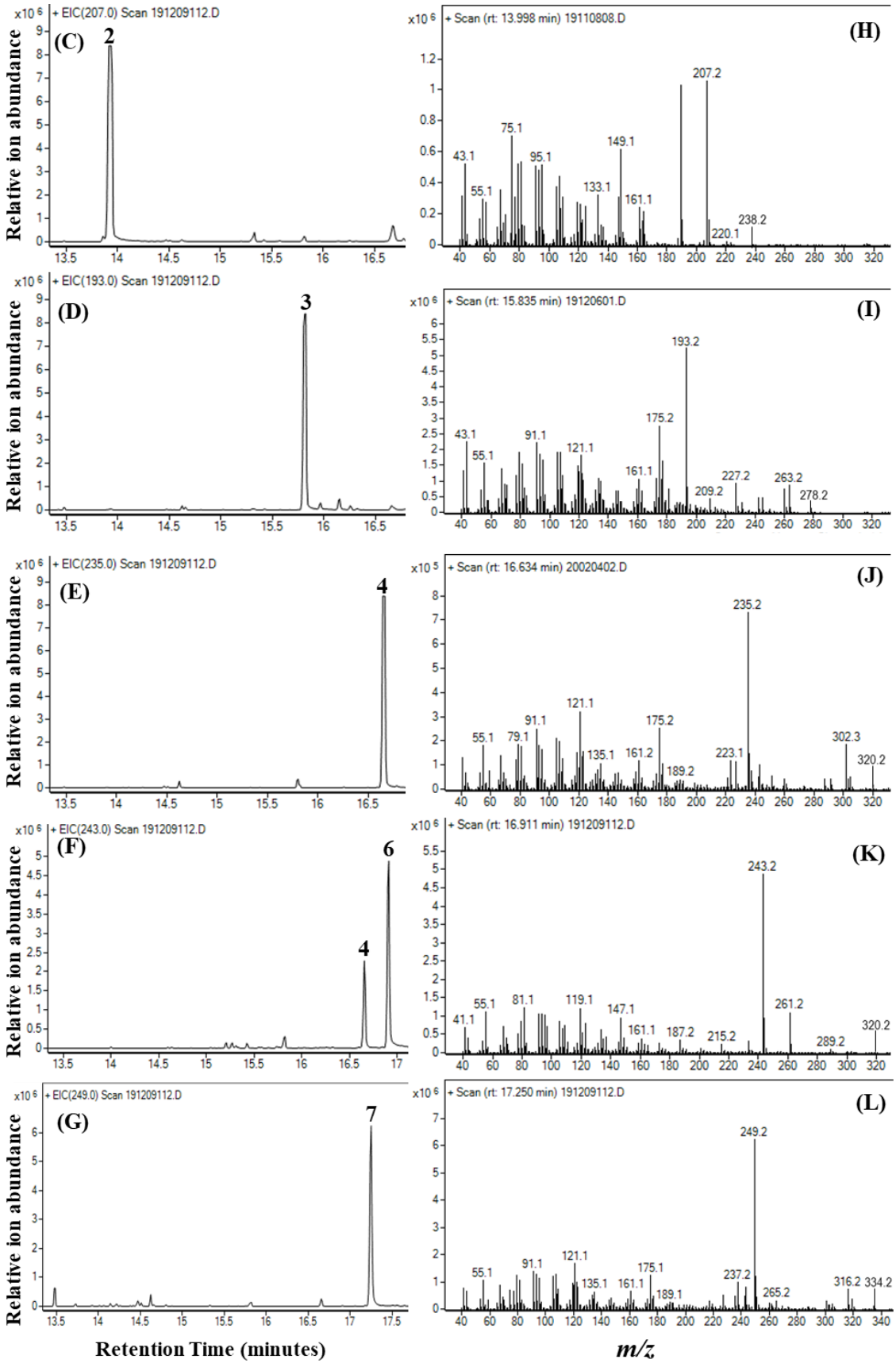
(C)
2
+ EIC(207.0) Scan 191209112.D
(H)
+ Scan (rt: 13.998 min) 19110808.D
(D)
3
+ EIC(193.0) Scan 191209112.D
(I)
+ Scan (rt: 15.835 min) 19120601.D
(E)
4
+ EIC(235.0) Scan 191209112.D
(J)
+ Scan (rt: 16.634 min) 20020402.D
(F)
6
4
+ EIC(243.0) Scan 191209112.D
(K)
+ Scan (rt: 16.911 min) 191209112.D
(G)
7
+ EIC(249.0) Scan 191209112.D
(L)
+ Scan (rt: 17.250 min) 191209112.D
Relative ion abundance
Retention Time (minutes)
m/z

Microbial-Elicited Accumulation of Novel Dolabralexins

Maize dolabralexin biosynthesis involves the sequential activity of type II and type I diterpene synthases namely, ZmAn2 and ZmKSL4 to form the C20 diterpene hydrocarbon dolabradiene (Figure 10) (Mafu *et al.* 2018). In maize, epoxydolabranol is of particular interest and significance given that it is among the single most potent antifungal agent against multiple pathogenic *Fusarium* species yet identified in plants (Mafu et al., 2018). As a related and shared defensive pathway branch, ZmAn2 and ZmKSL2 form the diterpene hydrocarbon *ent*-isokaurene which serves as the predominant precursor to the kauralexin class of acidic antibiotics (Ding *et al.* 2019). To understand if the newly discovered dolabralexins are also pathogen inducible, replicated planting of the maize inbreds were grown in the greenhouse side-by-side in pots containing either peat moss based commercial potting soil (BM2, Berger Corp. Canada) as a non-eliciting soil control or BFS field collected soil mixed 1:1 with BM2 soil. Across all maize lines grown in field soil, sesquiterpenoid and diterpenoid (including DDD, NDA, DHD, and DA) accumulation was observed to be significantly higher in roots compared to those from BM2 potting soil (Figure 2. A-F). While the precise microbial communities responsible remain unknown, our results a consistent with a dynamic interactive role for soil fungi in the elicited production of dolabralexins.

Antifungal activity of the Novel Dolabralexin, 15,16-dinor-dolabradiol

Following the purification and NMR based identification of 15,16-dinor-dolabradiol, we examined antifungal activity against *F. verticillioides* and *F. graminearum.* Paralleling previous results with trihydroxydolabrene (Mafu et al., 2018), 15,16-dinor-dolabradiol inhibited the growth of *F. verticillioides* in a dose dependent fashion (Figure 3A). In contrast, significant *F. graminearum* growth inhibition was not observed (Figure 3B). Despite the occurrence *F.*

verticillioides as a highly co-evolved and relevant root pathogen in maize (Bacon lab references), our results support roles for highly modified dolabralexins in providing structurally diverse functional defenses.

Figure 2. Microbial-Elicited Accumulation of Maize Sesqui- and Diterpenoids in Maize OH43 Roots. Compounds are consistently labeled throughout the study. GC/MS TIC of vapour phase extracted OH43 root tissues that were, A, microbially-elicited (grown in field soil) and B, non-elicited (grown in BM2 soil). Within panel A, compounds 1-14, labeled above, were identified base on retention time (RT) and mass spectrum comparison. Compound 1 is β-costic acid, 3 is DDD, 4 is NDA-ME, 5 is an uncharacterized diterpenoid, 6 is DHD, 7 is DA-ME and 8 is an uncharacterized diterpenoid, 9 is zealexin A1 methyl ester, 10 is zealexin B1 methyl ester, 11 is ZA5-ME, 12 is zealexin A2 methyl ester, 13 is kauralexin B1 methyl ester, and 14 is kauralexin B3 methyl ester. Within plots C-F, different letters (a–d) represent significant differences. Average (n= 4; ±SE) root tissue concentration (mg g^{-1} fresh weight [FW]) of DDD, DHD, DA-ME, and NDA-ME levels in the microbially-elicited and non-elicited roots of the maize lines OH43 (C), MoG (D), W22 (E), B73 (F) (Student's t test).

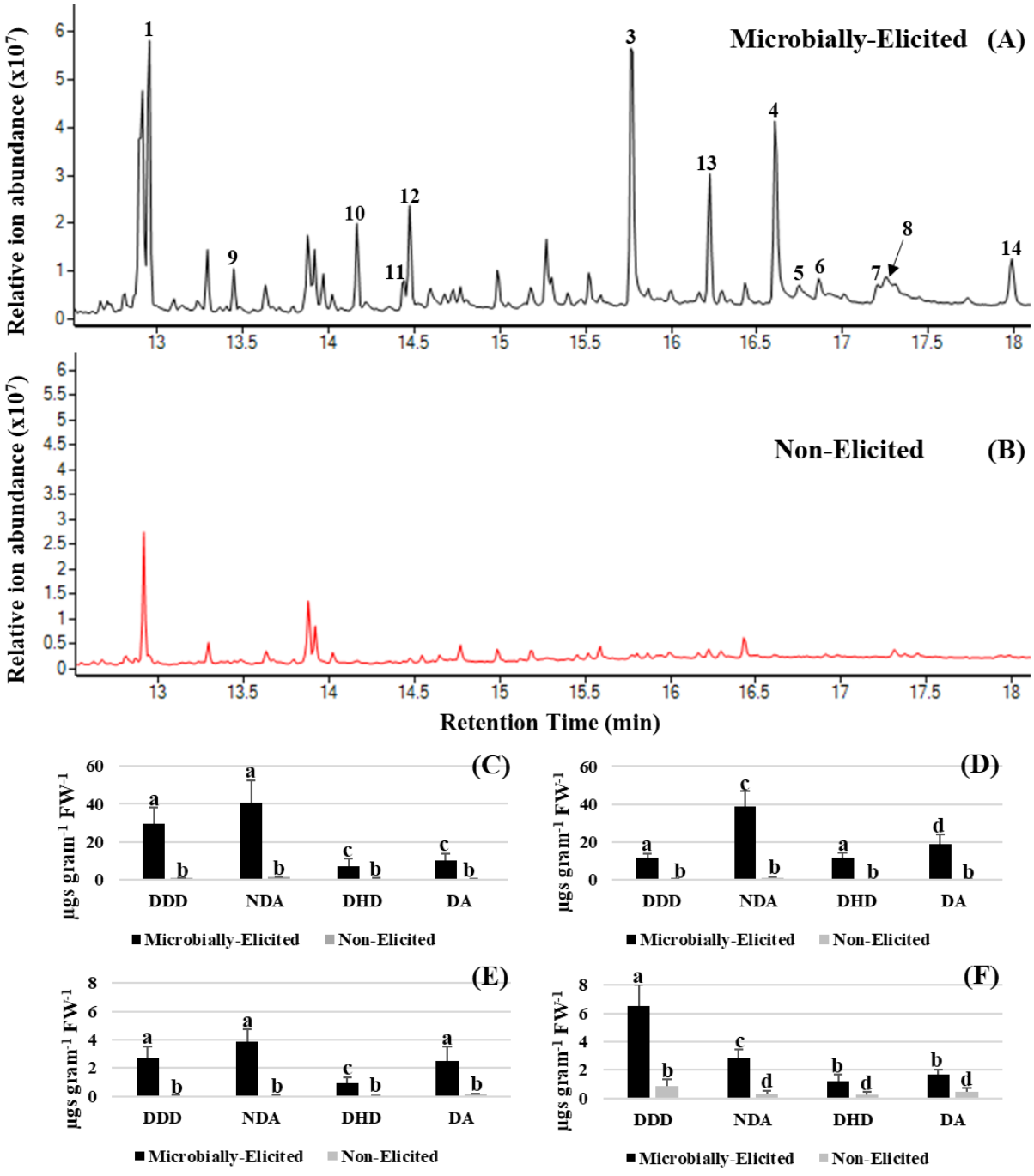
Microbially-Elicited (A)
Relative ion abundance (x10^7)
1
2
3
4
5
6
7
8
9
10
11
12
13
14
Non-Elicited (B)
Relative ion abundance (x10^7)
Retention Time (min)
(C)
µgs gram^-1 FW^-1
DDD
NDA
DHD
DA
Microbially-Elicited
Non-Elicited
(D)
µgs gram^-1 FW^-1
DDD
NDA
DHD
DA
Microbially-Elicited
Non-Elicited
(E)
µgs gram^-1 FW^-1
DDD
NDA
DHD
DA
Microbially-Elicited
Non-Elicited
(F)
µgs gram^-1 FW^-1
DDD
NDA
DHD
DA
Microbially-Elicited
Non-Elicited

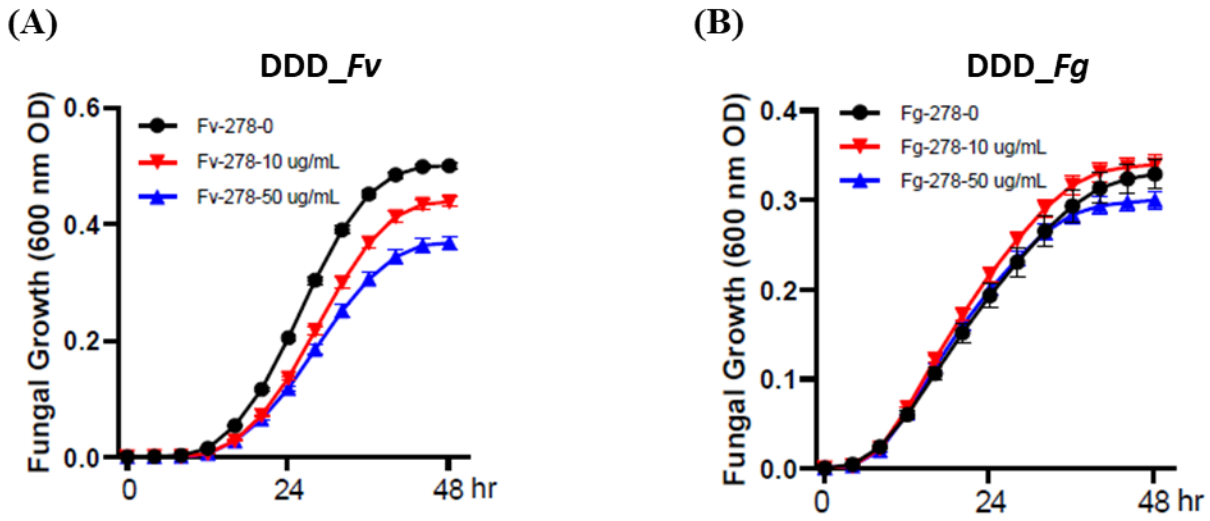

Figure 3. Antifungal Activity of DDD. DDD was previously termed compound 278. Average growth (OD_{600}) of F. verticillioides (A) and F. graminearum (B) is shown in the absence and presence of purified DDD measured over a 48-h time course in defined minimal broth medium using a microtiter plate assay.

Endogenous Support that DDD, NDA, DA and DHD are Downstream Products of Sequential Activity of ZmAn2 *and* ZmKSL4

To obtain endogenous confirmation that the novel dolabralexins are products of ZmAn2 and ZmKSL4, we analyzed the roots of *Zman2* and *Zmksl4* genetic mutants. Predictably, we were unable to detect significant root accumulation of the new dolabralexins in either *Zman2* or *Zmksl4* plants following growth in field soil. In contrast, the *Zmksl2* mutants and the wild type (WT) parents B73 (background for *Zmksl4* and *Zmksl2*) and W22 (background for *Zman2*) were found to accumulate all of the known dolabralexins supporting the predicted biosynthetic pathway (Figure 4. A-E).

Figure 4, Continued. *Zman2, and Zmksl4* Genetic Mutants Block Accumulation of DDD, NDA, DHD, and DA. GC/MS TIC of vapour phase extracted microbially-elicited root tissues of (A) *W22* (*WT*) Parent, and (B) Zm*an2* genetic mutant. DDD (compound 3) and NDA-ME (compound 4) identified at RT 15.77 min and 16.61min, respectively. Within plot C, different letters (a–e) represent significant differences. Average (n= 4; ±SE) concentration (mg g^{-1} fresh weight [FW]) of DDD, NDA, DHD, and DA levels in microbially-elicited root tissues of *Zman2*, *Zmksl2*, and *Zmksl4* genetic mutants and respective WT parent lines, W22 (*Zman2* WT parent line) and B73 (*Zmksl2* and *Zmksl4* WT parent line) (Student's t test).

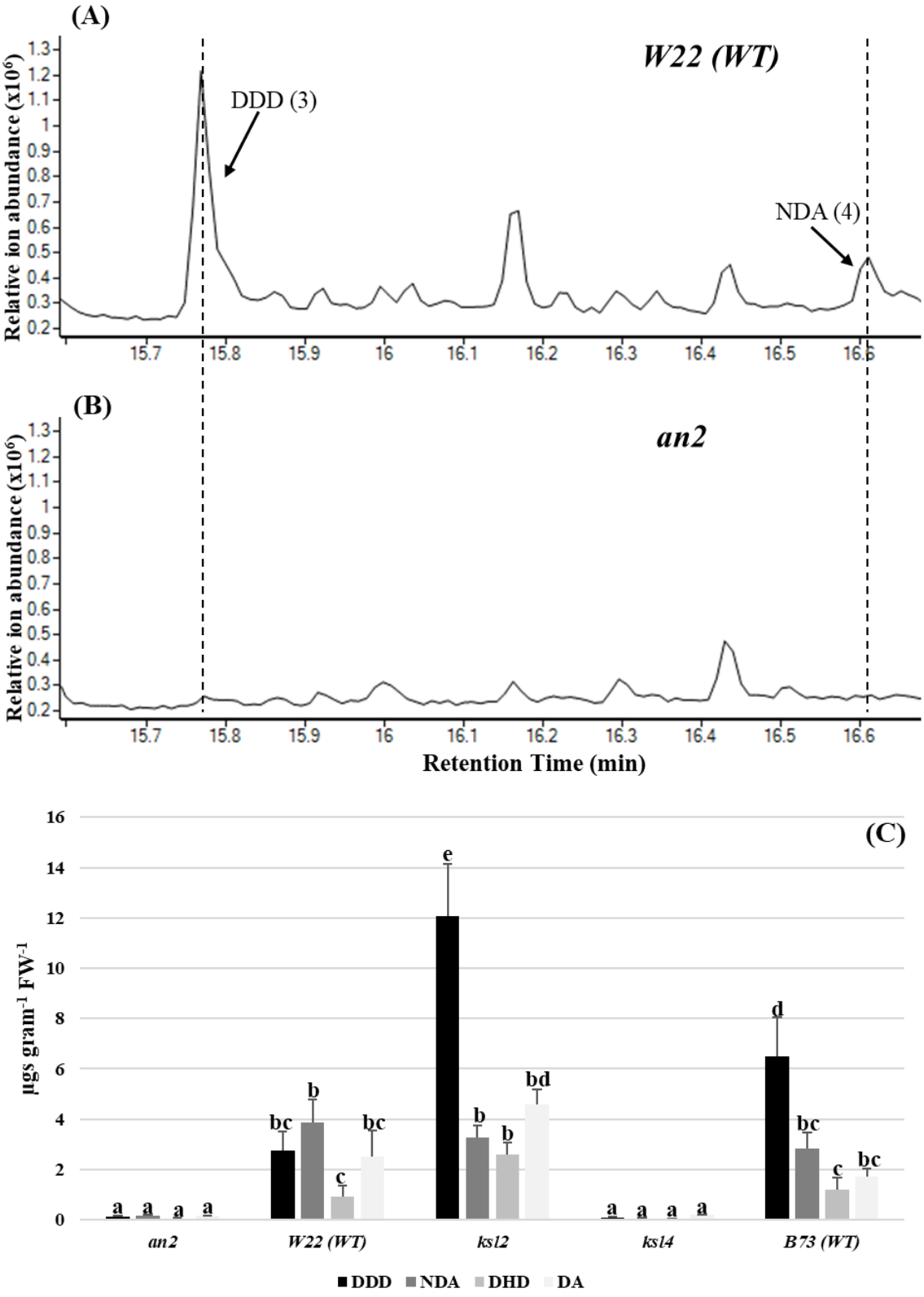
(A)
W22 (WT)
DDD (3)
NDA (4)
Relative ion abundance (x10^6)
(B)
an2
Retention Time (min)
(C)
µgs gram^-1 FW^-1
an2
W22 (WT)
ksl2
ksl4
B73 (WT)
DDD
NDA
DHD
DA

ZmCYP71Z16 Drives Dolabralexin Biosynthesis but may further directly contribute to the production of novel dinor-dolabralexins

We performed *Agrobacterium*-mediated transient overexpression enzyme assays in *Nicotiana benthamiana* (*N.b.*) using different combinations of ZmAn2 and ZmKSL4 with cytochrome (CYP) P450 monooxygenases (ZmCYP71Z19/18/16) known to function in the biosynthesis of maize terpenoid antibiotics (Mafu et al., 2018; Ding et al., 2019; Ding et al., 2020). Heterologous expression of *ZmAn2* + *ZmKSL4* genes with either *ZmCYP71Z18*, *ZmCYP71Z19*, or *ZmCYP72A358* (i.e. GRMZM2G147742) resulted in levels of 15,16-dinor-dolabradiol (DDD) and 16-nordolabranolic acid (NDA) not significantly different from background levels of abundance present from the *ZmAn2*/*ZmKSL4* pair alone (Fig. 6. B). Expression of the *ZmAn2/ZmKSL4* pair with either *ZmCYP71Z16* alone or further additive combinations including either *ZmCYP72A358* (i.e. GRMZM2G147742) or *ZmCYP71C60* (i.e. GRMZM2G399530) are consistent with the production of significantly increased levels of the DDD and NDA-ME compared to *ZmAn2/ZmKSL4* alone (Fig. 5. G). Given that *ZmCYP72A358* (i.e. GRMZM2G147742) and *ZmCYP71C60* (i.e. GRMZM2G399530) have only a modest impact (if any) on DDD and NDA-ME levels resulting from the *ZmAn2/ZmKSL4/ZmCYP71Z16* co-expression alone, we hypothesize that ZmCYP71Z16 may contribute to the production of complex dolabralexin products possibly by again continuing to perform oxidation reactions after epoxydolabranol is converted to trihydroxydolabrene by endogenous epoxide hydrolases. (Figures 5 and 6) (Mafu et al., 2018).

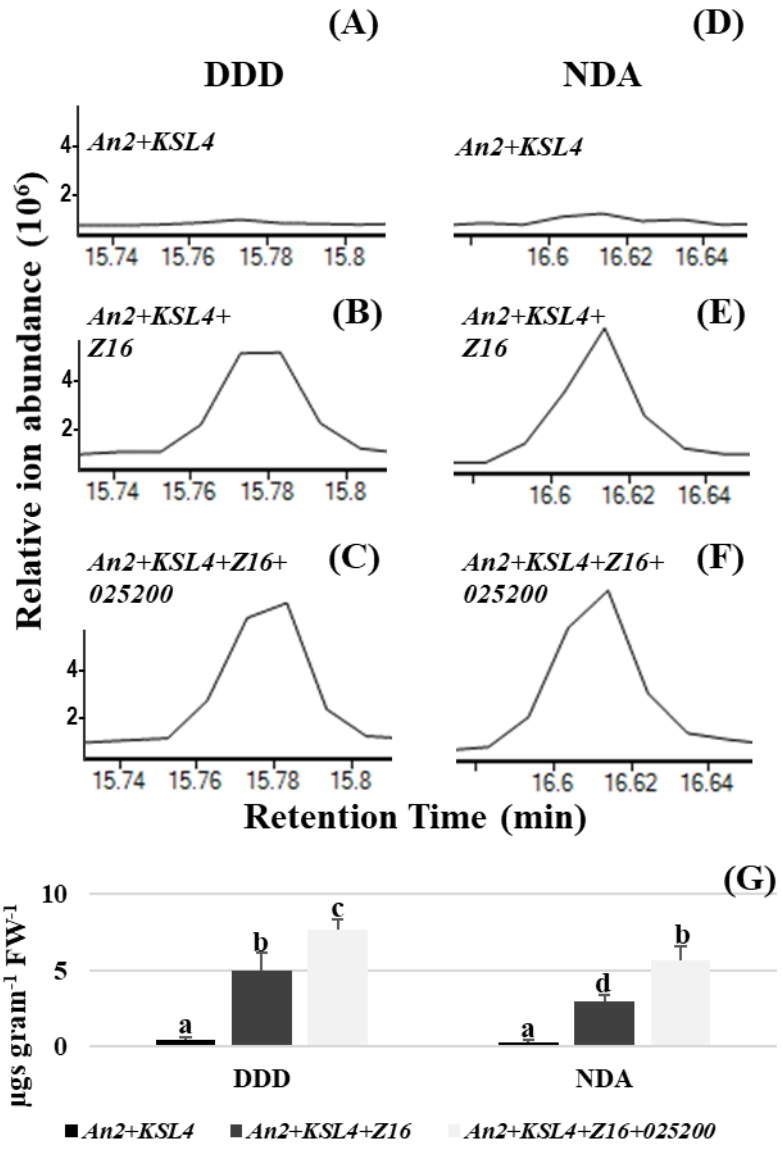

Figure 5. ZmCYP71Z16 May Contribute to The Production of Complex Dolabralexin Products Beyond Epoxydolabranol. A-F, GC/MS EIC are shown for leaf tissue VPE of Agrobacterium-mediated transient *N. benthamiana* overexpression assay of the gene constructs *An2+KSL4*, *An2+KSL4+Z16*, and *An2+KSL4+Z16+025200*, Top to bottom. Left panels show DDD peaks while the right panels show NDA-ME peaks. Within plot G, different letters (a–d) represent significant differences. Average (n= 4; ±SE) root tissue concentration (mg g-1 fresh weight [FW]) of DDD, and NDA-ME levels in Agrobacterium-mediated transient *N. benthamiana* expression assay tissues expressing gene constructs *An2+KSL4*, *An2+KSL4+Z16* and *An2+KSL4+Z16+025200* (Student's t test).

Figure 6. Comparative Analysis of Agrobacterium-Mediated Transient N. benthamiana Overexpression Assays Provides Supports for Z16 Role in Dolabralexin Pathway. GC/MS bases quantifications are shown for leaf tissue VPE of Agrobacterium-mediated transient *N. benthamiana* overexpression assay of the gene constructs *An2+KSL4*, *An2+KSL4+Z16*, *An2+KSL4+Z18*, *An2+KSL4+Z19*, *An2+KSL4+147774*, *An2+KSL4+Z16+147774*, and *An2+KSL4+Z16+*025200. Within plots A and B, different letters (a–e) represent significant differences. A, Average (n= 4; ±SE) root tissue concentration (mg g-1 fresh weight [FW]) of epoxydolabrene, and epoxydolabranol levels in Agrobacterium-mediated transient *N. benthamiana* overexpression assay tissues (Student's t test). B, Average (n= 4; ±SE) root tissue concentration (mg g-1 fresh weight [FW]) of DDD, and NDA-ME levels in Agrobacterium-mediated transient *N. benthamiana* overexpression assay tissues (Student's t test).

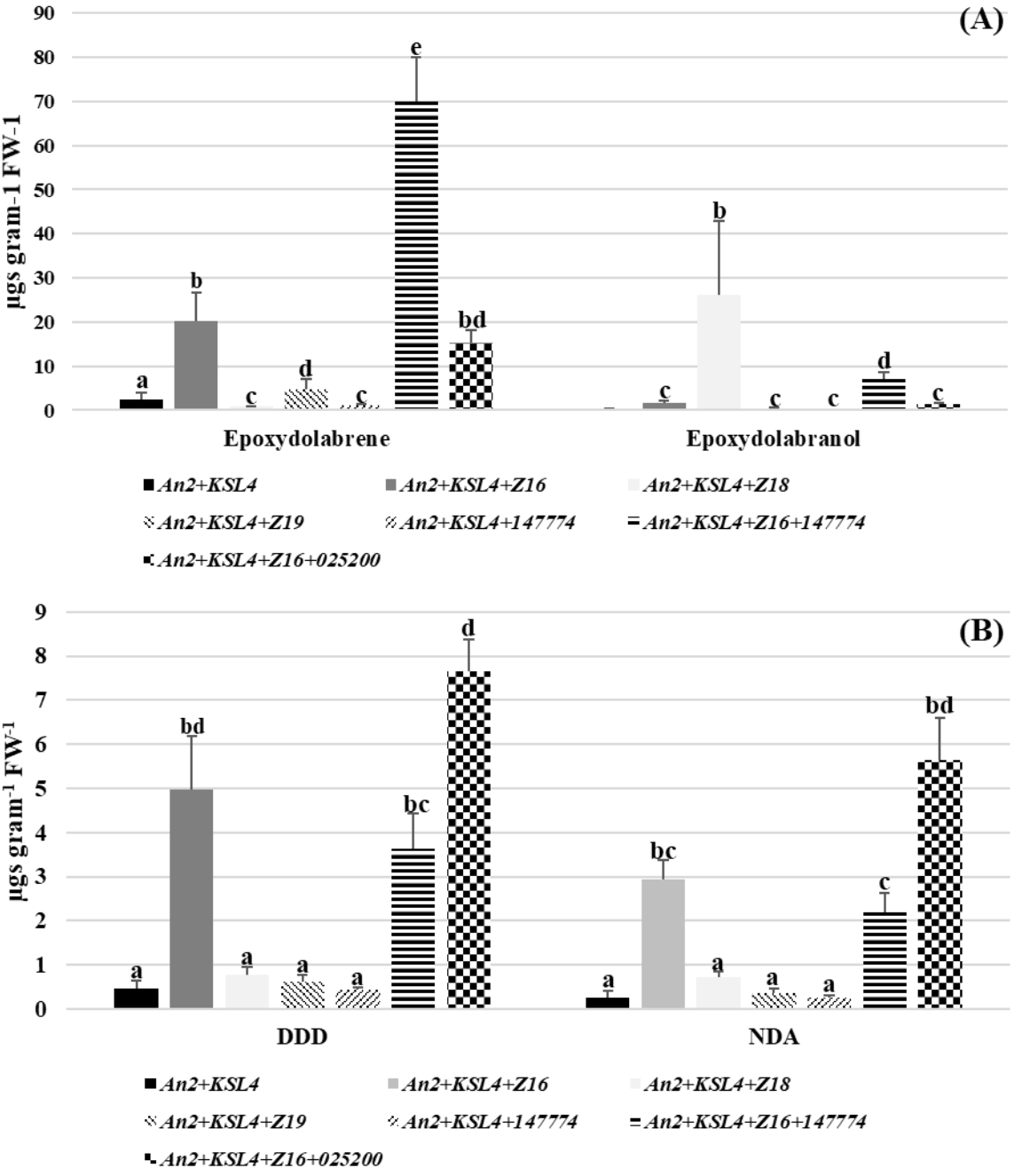

Forward Genetic Mapping Experiments Support the Existence of Genes Regulating the Dolabralexin Pathway on Chromosome 5

In addition to the *N.b.* transient expression assays, we performed chemical analyses on maize roots harvested from field grown plants using a biparental PHW65 x MoG Recombinant Inbred Line (RIL) mapping population (Gage et al., 2018) and the Goodman diversity panel

(Flint-Garcia *et al.* 2005) in effort to generate additional P450 candidates in the dolabralexin pathway using forward genetics and association mapping. GC/MS analyses conducted on the individual parent lines, namely MoG and PHW65, showed dramatic differences in metabolite levels encouraging complete analysis of the whole population alongside the Goodman panel (Figure 7. A-F). Following GC/MS analyses, we performed metabolite ratio mapping in both the association panel and biparental datasets. Using epoxydolabranol alone as a metabolite mapping trait in the PHW65 x MoG RIL population, the most statistically significant SNP was located at Chromosome 5 position 25,546,627 (B73_RefGen3). Given that epoxydolabranol is a parsimonious precursor to the novel dolabralexins reported in this thesis we conducted further mapping trials using ratios as follows: dihydroxydolabrone (DHD)/epoxydolabranol (Figure 8B); 15,16-dinor-dolabradiol (DDD)/ epoxydolabranol (Figure 8C); 16-nordolabranolic acid (NDA)/ epoxydolabranol (Figure 8D); and dolabranolic acid (DA)/epoxydolabranol (Figure 8E). Given the observed decreases in $-\log_{10}(P)$ values denoting further increases in statistical significance on chromosome 5 we interpret the results to support the presence of gene most influencing the precursor/product relationships of epoxydolabranol to dolabranolic acid (DA) (Fig. 8F). To consider new dolabralexin pathway gene candidates on chromosome 5, we utilized global gene co-expression analyses using Mutual Rank (MR) scores for genes in the mapping interval (Figure 9. A, B). Using *ZmKSL4* expression to guide the MR mapping interval interrogation, we observed co-expression with a CYP P450 monooxygenase (*ZmCYP89A6, Zm00001d014335*) and *Zm00001d013934* (epoxide hydrolase) in addition to previously observed co-expression with *ZmCYP71Z19* and *ZmCYP71Z16* (Figure 9A). Additional MR analyses using the candidate gene *ZmCYP89A6* and MR co-expression with all genes in the B73 genome, indicate that *ZmCYP89A6* is associated with defense metabolism specifically diterpenoid defense, due to the

fact that 6 of the 8 top co-expressed genes namely, *ZmAn2* (*Zm00001d029648*), *ZmKSL2* (*Zm00001d041082*), *ZmKR2* (*Zm00001d018847*), *ZmKO2* (*Zm00001d046342)*, *GGPP* (geranylgeranyl pyrophosphate, *Zm00001d021929*) *Synthase,* and *ZmKSL4* are known to code for enzymes that catalyze core enzymatic steps of maize diterpenoid defense metabolite biosynthesis**.** Collectively the chemical analyses of B73/W22 wildtype and defined genetic mutants (*Zman2, Zmksl4,* and *Zmksl2*) coupled with *N.b.* transient expression assays, metabolite-based association mapping, and MR analyses led us to the current pathway model for an expanded family of maize dolabralexin antibiotics (Figure 10).

Figure 7, Continued. Microbially-Elicited Root Tissues of Biparental Mapping Population PHW65 and MoG Parent Lines Exhibit Varying Levels of DDD and NDA. GC/MS TIC of vapour phase extracted root tissues of, (A) MoG, (B) PHW65, (C) PM-RIL-156, (D) PM-RIL-354 that were microbially-elicited. Within plot E, asterisks (***) represent significant differences. Average (n= 4; ±SE) fold increase in root tissue concentration (mg g^{-1} fresh weight [FW]) of DDD, and NDA-ME levels in the microbially-elicited MoG parent line relative to PHW65 (Student's t test). Within plot F are concentration (mg g^{-1} fresh weight [FW]) of DDD, NDA, DHD, DA, compounds 5 and 8, other previously characterized dolabralexins, costic acid, kudtdiol (compound 2) and the sum of all known dolabralexin, kauralexin and zealexin levels in microbially-elicited root tissues of PM-RIL-156 and PM-RIL-354.

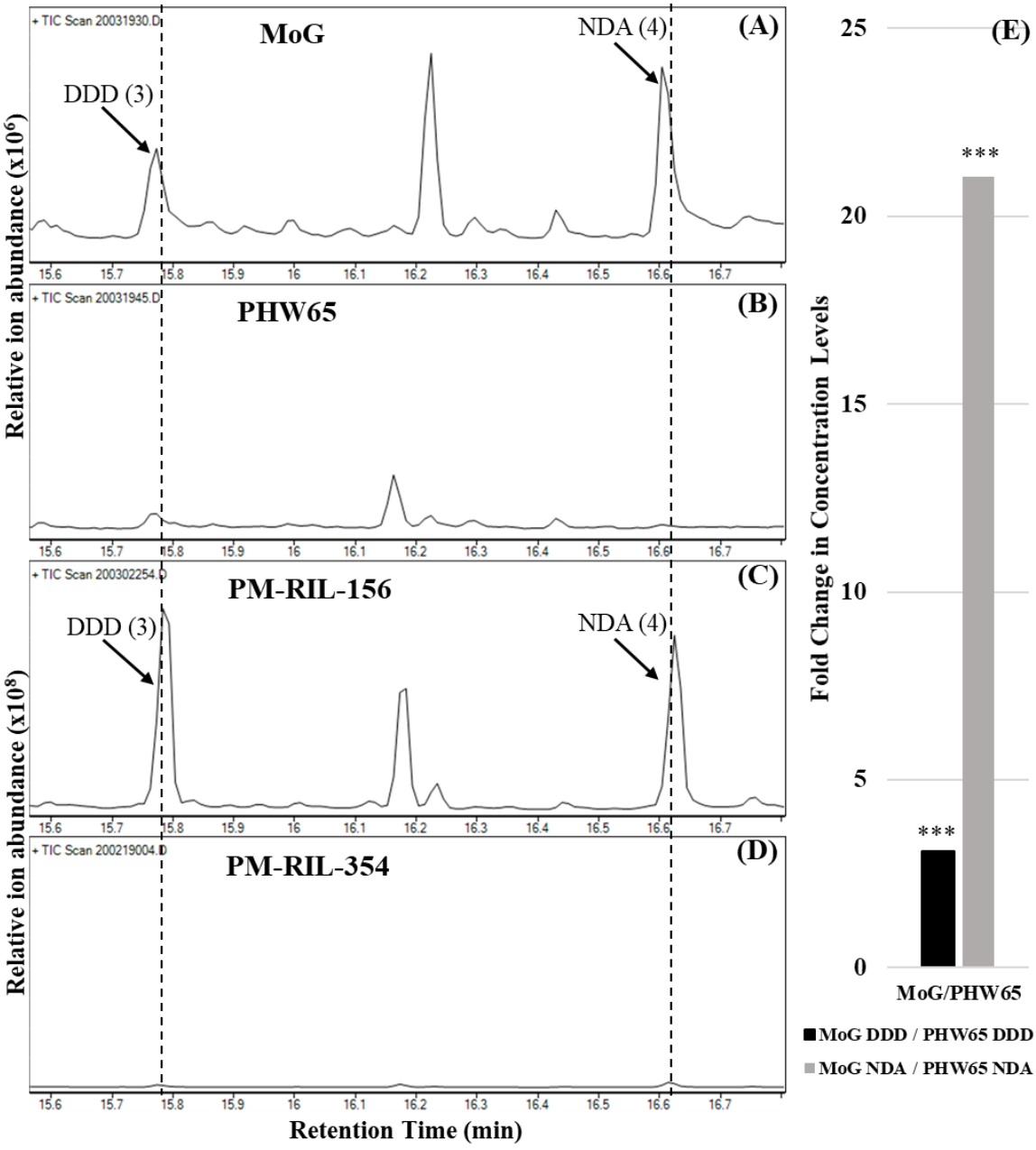
+ TIC Scan 20031930.D
MoG
(A)
DDD (3)
NDA (4)
+ TIC Scan 20031945.D
PHW65
(B)
+ TIC Scan 200302254.D
PM-RIL-156
(C)
DDD (3)
NDA (4)
+ TIC Scan 200219004.D
PM-RIL-354
(D)
Relative ion abundance (x10⁶)
Relative ion abundance (x10⁸)
15.6 15.7 15.8 15.9 16 16.1 16.2 16.3 16.4 16.5 16.6 16.7
Retention Time (min)
(E)
Fold Change in Concentration Levels
25
20
15
10
5
0
***
***
MoG/PHW65
MoG DDD / PHW65 DDD
MoG NDA / PHW65 NDA

(F)	Compound Concentration Levels (µgs gram^{-1} FW$^{-1)}$	
Compound	**PM-RIL-156**	**PM-RIL-354**
Dolabradiene	37	1
Dolabranol	1423	15
Epoxydolabrene	12	0
Epoxydolabranol	41	0
DDD	1805	13
NDA	2155	58
Compound 5	154	8
DHD	862	8
DA	775	14
Compound 8	80	3
All Dolabralexins	7345	120
All Kauralexins	2913	88
All Zealexins	6857	2656
Costic Acid	3185	1255
Kudtdiol	2726	131

Figure 8, Continued. Forward Genetic Mapping Experiments Support the Existence of Genes Regulating the Dolabralexin Pathway on Chromosome 5. Within plots A-E, PHW65 x MoG biparental root metabolite mapping using epoxydolabranol (A), and ratios of DHD (B), DDD (C), NDA-ME (D) and DA-ME (E) separately to epoxydolabranol as mapping traits reveals the top SNP (single nucleotide polymorphism) at 24,423,963 (B73_RefGen3) on chromosome 5. ZmCYP71Z16 (Zm00001d014136) is located at Chromosome 5 position 33,743,814 which is within 100 genes of SNP 24,423,963 (B73_RefGen3). Graphed in plot E are the $-\log_{10}$(P-values) vs. SNPs found in chromosome 5 for each mapping trait. Additionally, within Plot E figure legend are visual representations of the mapping traits used.

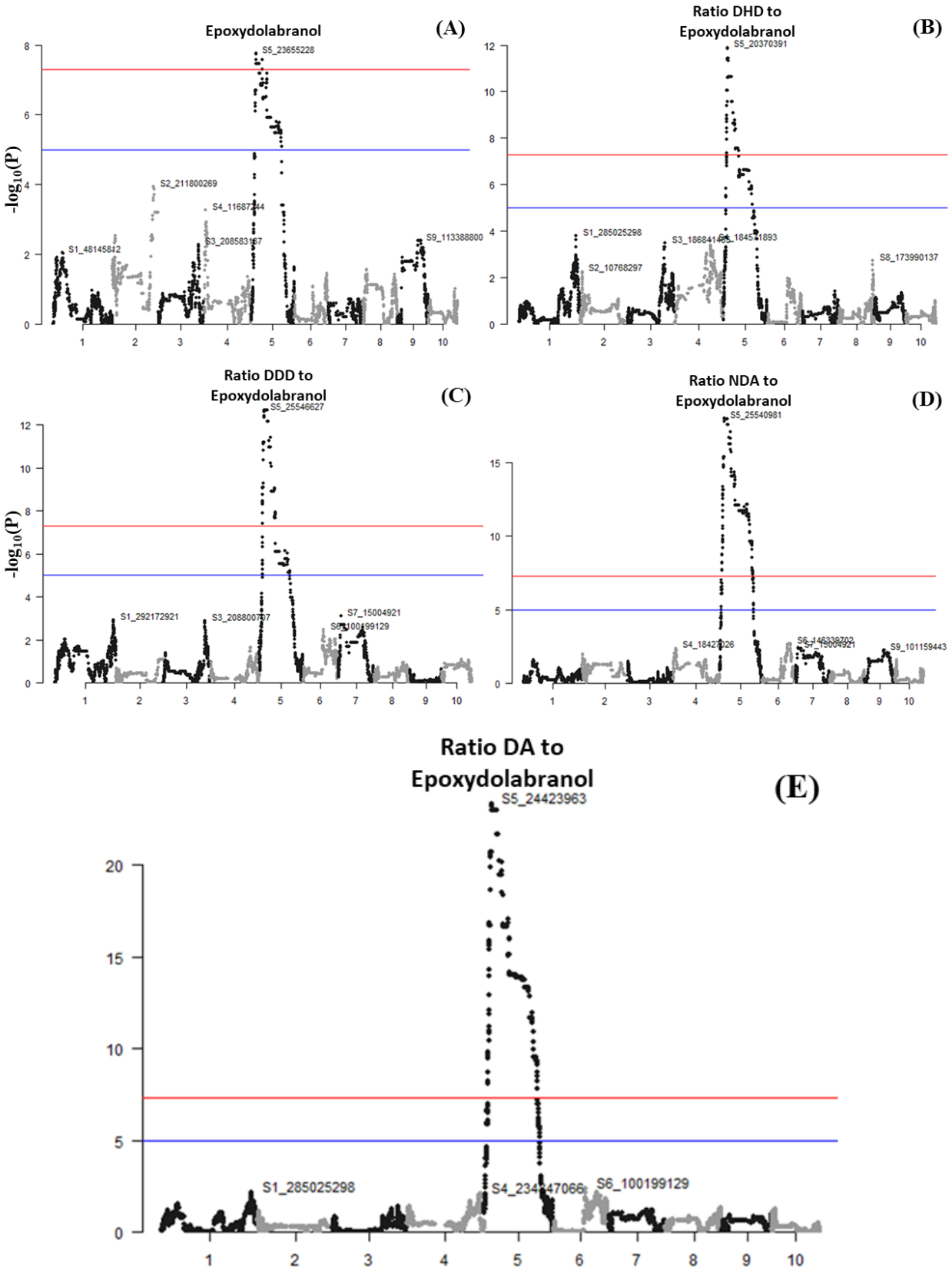
Epoxydolabranol
(A)
S5_23655228
S2_211800269
S4_116872144
S3_208583167
S1_48145842
S9_113388800
-log10(P)
Ratio DHD to Epoxydolabranol
(B)
S5_20370391
S1_285025298
S2_10768297
S8_173990137
Ratio DDD to Epoxydolabranol
(C)
S5_25546627
S1_292172921
S3_208800797
S7_15004921
S6_100199129
Ratio NDA to Epoxydolabranol
(D)
S5_25540981
S4_184228026
S9_101159443
Ratio DA to Epoxydolabranol
(E)
S5_24423963
S1_285025298
S4_234247066
S6_100199129

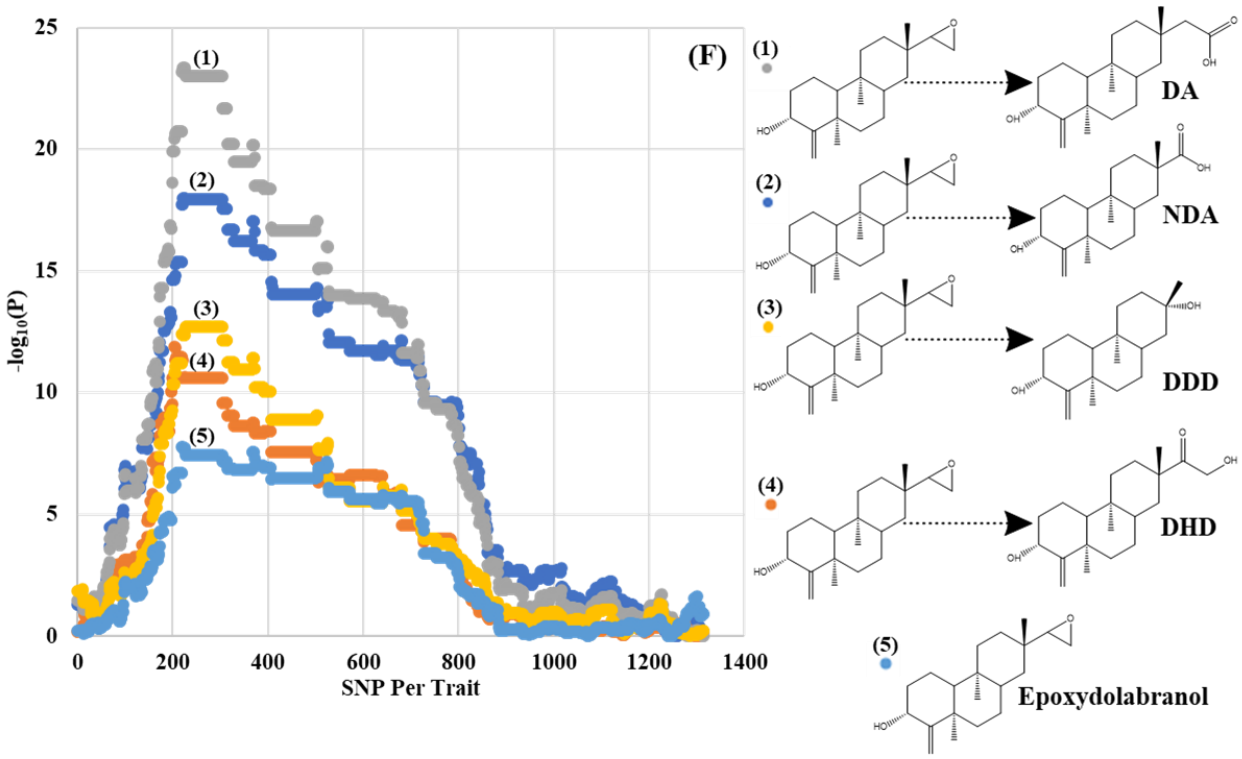
(F)
(1)
(2)
(3)
(4)
(5)
25
20
15
10
5
0
-log10(P)
0
200
400
600
800
1000
1200
1400
SNP Per Trait
DA
NDA
DDD
DHD
Epoxydolabranol

Figure 9. Global Gene Co-Expression Analysis Using Mutual Ranks Reveals ZmCYP89A6 as a Candidate Involved in Dolabralexin Pathway Regulation. Maize (B73_RefGen4) Kremling Qteller RNA sequence data used in producing the mutual rank scores. Low numbers indicate supportive mutual rank (MR) scores. Genes in panels A and B were each identified and selected from a pool of 100 co-expressed genes. A, Heat map depicting the co-expression of genes, *KSL4* (*Zm00001d032858*), *Z19* (*Zx5*, *Zm00001d014121*), *Z16* (*Zx7*, *Zm00001d014136*), *ZmCYP89A6* (*Zm00001d014335*) and an *epoxide hydrolase* (*Zm00001d013934*). B, A, Heat map depicting the co-expression of genes, *ZmCYP89A6*, *Z18* (*Zx6*, *Zm00001d014134*), *An2* (*Zm00001d029648*), *KSL2* (*Zm00001d041082*), *KR2* (*Zm00001d018847*), *KO2* (*Zm00001d046342*), *ZmCYP86A1*(*Zm00001d042814*), *GGPP* (geranylgeranyl pyrophosphate, *Zm00001d021929*) *Synthase*, *KSL4*.

(A)	*KSL4*	*Zx7*	*Zx5*	*ZmCYP89A6*	*Epoxide Hydrolase*
KSL4					
Zx7	28				
Zx5	98	106			
ZmCYP89A6	119	1206	145		
Epoxide Hydrolase	215	566	118	347	

(B)	*ZmCYP89A6*	*Zx6*	*An2*	*KSL2*	*KR2*	*KO2*	*ZmCYP86A1*	*GGPP Synthase*	*KSL4*
ZmCYP89A6									
Zx6	9								
An2	13	2							
KSL2	27	2	3						
KR2	37	8	21	28					
KO2	87	16	5	6	151				
ZmCYP86A1	94	48	93	178	19	390			
GGPP Synthase	100	18	14	164	113	386	37		
KSL4	119	121	19	40	111	6	929	1455	

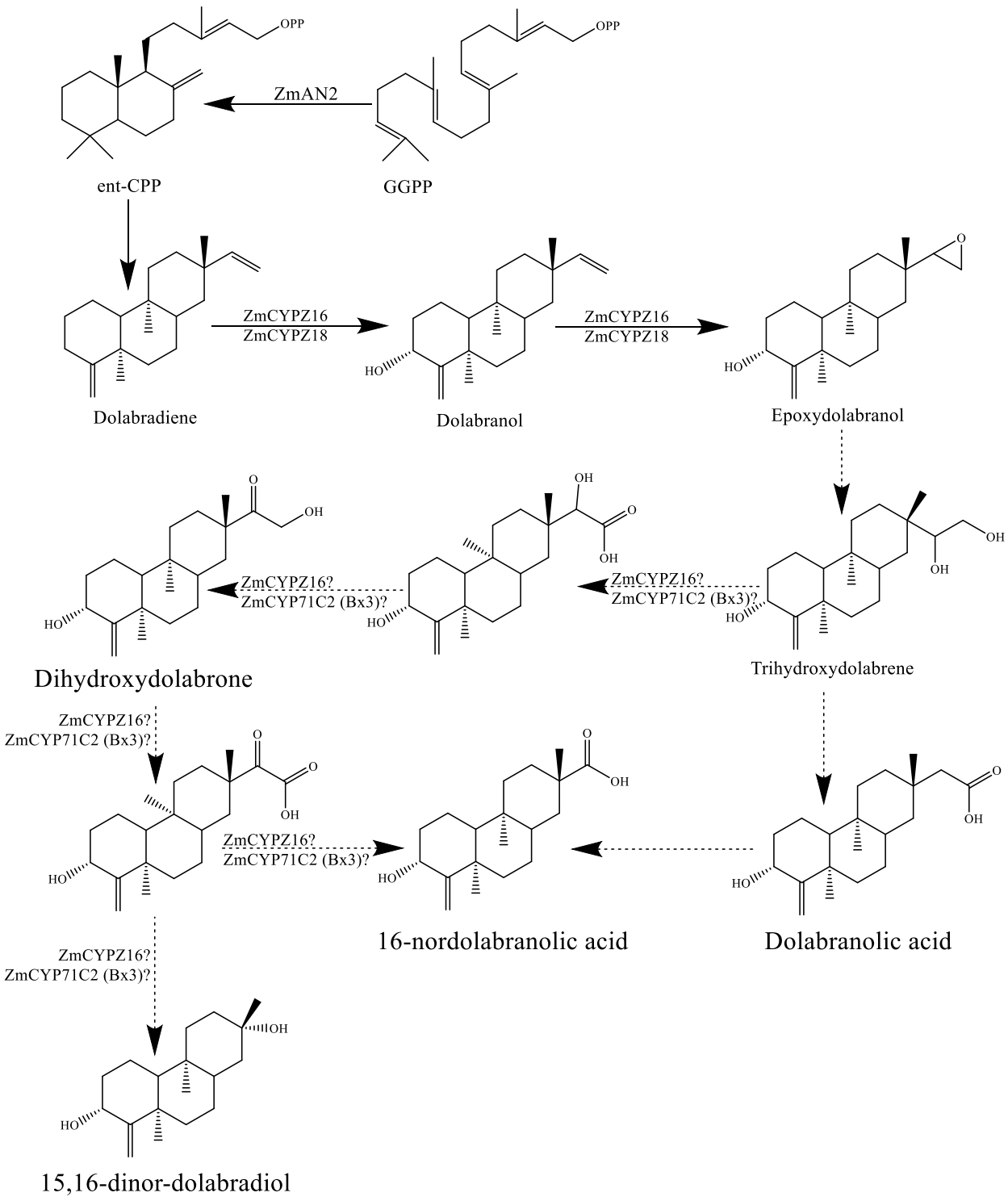

Figure 10. Maize Dolabralexin Pathway. Dashed arrows represent undefined enzymatic steps without labels. Dashed arrows with labels represent enzymatic steps supported by genetics and N.b. transient overexpression assays.

Table 1. Genes List of *Agrobacterium*-mediated transient overexpression enzyme assays in *Nicotiana benthamiana* (*N.b.*). Corresponding known Version 3, Version 4, Zx and common names for relevant zealexin, and dolabralexin pathway terpenes synthases and cytochrome P450's.

Gene_V3	Gene_V4	Gene Name	Protein Product
GRMZM2G122654	Zm00001d014121	*Zx5*	CYP71Z19/Zx5
N/A	Zm00001d014134	*Zx6*	CYP71Z18/Zx6
GRMZM2G067591	Zm00001d014136	*Zx7*	CYP71Z16/Zx7
GRMZM2G044481	Zm00001d029648	*ZmAn2*	An2
GRMZM2G016922	Zm00001d032858	*ZmKSL4*	KSL4
GRMZM2G147774	Zm00001d044147	*ZmCYP72A358*	CYP72A358
GRMZM2G399530	Zm00001d025200	*ZmCYP71C60*	CYP71C60

Table 2. Gene List of Maize *Zman2, Zmksl2 and Zmksl4* Mutant Lines. B73 is the WT parent for *Zmksl4/Zmksl2 and* W22 is the WT parent for *Zman2*.

Gene_V3	Gene_V4	Gene Name	Protein Product	Wild Type (WT) Parent Line
GRMZM2G044481	Zm00001d029648	*ZmAn2*	An2	B73
AC214360.3_FG001	Zm00001d041082	*ZmKSL2*	KSL2	W22
GRMZM2G016922	Zm00001d032858	*ZmKSL4*	KSL4	W22

Table 3. Data Sets Used in the Production of Figures. In this study, Mutual Ranks are correlation analyses of transcripts.

Data Set	**Description**
Goodman Diversity Panel (Metabolomic)	~300 Maize lines representative of all maize pedigree were field grown. 38day old root tissue VPE were performed for all lines and analyzed by EI-GC/MS.
Biparental PHW65 x MoG Recombinant Inbred Lines (RIL) Mapping Population (Metabolomic)	~180 genome sequenced PHW65xMoG RILs were field grown. 40day old root tissue VPE were performed for all lines and analyzed by EI-GC/MS.
Maize Version 4 Kremling Qteller RNA Sequence (Transcriptomic)	Kremling *et al*. (2018) produced multi-tissue gene expression resource that represents the genotypic and phenotypic diversity of modern inbred maize, and includes transcriptomes in an average of 255 lines in seven tissues. Data set used for global gene co-expression analyses using Mutual Rank scores.
Agrobacterium-mediated transient overexpression enzyme assays in *N.b.* (Metabolomic)	6-week-old *N.b.* plants were Agrobacterium infiltrated with different combinations of ZmAn2 and ZmKSL4 with cytochrome (CYP) P450 monooxygenases. Leaf tissues were harvested 5 days post infiltration. Subsequently, leaf tissues were VPE and analyzed by EI-GC/MS.
Maize Diterpene Synthase Genetic Mutants (Metabolomic)	W22 and B73 maize lines were used to produce *Zman2, Zmksl2,* and *Zmksl4,* genetic mutants. Plants were greenhouse grown in field/BM2 soil. 30day old root tissue VPE were performed for all lines and analyzed by EI-GC/MS.

Discussion

The goal of this effort was to identify novel defense metabolites and their corresponding biosynthetic pathways to understand basic biochemical mechanisms maize relies on for survival in large scale monocultures increasing relied on by humans. An understanding and optimization of maize protective biochemicals that impede pest and pathogen attack will be essential to mitigate significant yield losses that could compromise our global economy. To uncover additional maize defenses, we worked to broaden scope of detectable analytes observable by GC/MS. This was achieved by a large number of simple modifications of existing VPE sample preparation methods that now avoid chemical contamination at every step and ultimately achieve a two-fold increase in the number of previously detectable analytes. Improved sample preparation for GC/MS analyses coupled with HPLC based purifications of optimal maize tissue resulted in the elucidation of the 4 new members of the dolabralexin pathway.

In all of our analyses thus far, the four new dolabradiene derived metabolites seem to only be detected in microbially elicited root tissues (Fig 2). Comparing panels, A and B from figure 2, we can see a dramatic difference in the number and size of peaks in the TIC. None of the labeled metabolites are found in any significant levels in these tissues. Looking at panels C-F which have quantifications of the novel dolabralexins, we can see that for each maize line, the non-elicited tissues have significantly lower concentration levels of the metabolites compared to the microbially-elicited tissues. Although there are huge differences in the metabolite concentrations between different maize lines, which probably accounts for the forward genetic mapping results (Fig 8), but within each maize line the patterns of abundance remain constant. Supporting the idea of pathogen inducibility of at least one of the novel metabolites is gained by observing the antifungal activity DDD exhibit against *Fv* (Fig 3A). DDD significantly inhibits

the growth of *Fv*, a root specific fungus, and does not significantly inhibit *Fg*, a stem specific fungus (Fig 3). This completely aligns with all data we have gathered so far in that these metabolites are inducible, and only present in root tissues, thus will be *de novo* produced to specifically fight against root pathogens.

Knowing that ZmAn2 and ZmKSL4 are sequential producers of dolabradiene and that comparative structural analysis reveals a significant level of similarity between the four new metabolites and dolabradiene, we examined existing *Zman2, and Zmksl4* genetic mutants to test for the possibility that these metabolites are dolabradiene derived. Elicited root tissues of *Zman2, and Zmksl4* plants confirmed deficiency in the novel metabolites while all detectable dolabralexins were present in wildtype parents, thus, providing evidence that the novel dolabralexins are products of ZmAn2 and ZmKSL4 (Fig 4).

Analyses of tissues of *Agrobacterium*-mediated transient overexpression enzyme assays in *N. benthamiana* using combinations of the ZmAn2 and ZmKSL4 pair with separate cytochrome (CYP) P450 monooxygenases (ZmCYP71Z19/18/16) produced some unusual results. Specifically, Mafu et al. (2018) previously established that both ZmCYP71Z16 and ZmCYP71Z18 had the ability to convert dolabradiene to epoxydolabranol. In our assays, we partially confirmed this result and found that the combination of ZmAn2 + ZmKSL4 + ZmCYP71Z18 resulted in the accumulation of detectable epoxydolabranol in tobacco tissues (Fig. 6A). Curiously, we only observed NDA and DDD accumulation when ZmAn2 + ZmKSL4 + ZmCYP71Z16 enzymes were co-expressed. This result was largely independent of the presence and absence of additionally examined P450s (Fig. 6B). We hypothesize that upon opening of the epoxide ring on epoxydolabranol to trihydroxydolabrene, it might be possible that ZmCYP71Z16 specifically, but not ZmCYP71Z18, is able to continue further oxidative reactions

such as conversion of the terminal alcohol on trihydroxydolabrene to a carboxylic acid as found on dolabranolic acid. Further activities are required to reach DDD and NDA as observed in *N. benthamiana* (Fig 6B) tissues and it must be emphasized that the interaction of native *N. benthamiana* enzymes cannot be ruled out and would require analyses using purified enzymes. However, the question arises, could ZmCYP71Z16 be directly involved in not only oxidative reactions but also the further decarboxylation reactions which would be required to generate the 19C compound 16-nordolabranolic acid (NDA) and the C18 compound 15,16-dinor-dolabradiol (DDD). One well characterized example from the literature is the mammalian enzyme CYP17A1 displays both 17α-hydroxylase activity and 17,20-lyase activity on human progestogens such as pregnenolone to create a tertiary C17 alcohol and then 17,20 lyase activity that yields a 2-carbon loss generating the androgen dehydroepiandrosterone (DeVore and Scott EE, 2012). While conceptually useful it should be noted that this reaction mechanism is not perfectly compatible with the key carbon 13 position of dolabradiene as the formation of a tertiary C13 alcohol is not possible at a quaternary carbon. Thus, if occurring, additional speculative reaction mechanisms of ZmCYP71Z16 in the dolabradiene pathway would provide new and unexpected reaction mechanism insights.

In the process of discovering the structures and corresponding chemical configurations of the new metabolites in collaboration with Dr. Molinski (UCSD Molinski Lab), we were able to correct stereochemical configurations of dolabradiene and its downstream oxidative products (epoxydolabrene, epoxydolabranol, trihydroxydolabrene) found in "*Discovery, biosynthesis and stress-related accumulation of dolabradiene-derived defenses in maize*" (Mafu et al., 2018). Corresponding authors were contacted and an *erratum* was submitted. The corrected stereochemical configuration are as found in figure 10. Support for the stereochemistry

configuration correction, specifically for DDD is found in "*Isolation, Structure Elucidition, and Immunosuppressive Activity of Diterpenoids from Ligularia fischeri*," a Journal of Natural Products article (Gobu *et al.*, 2017). Detailed in this publication are the isolations, structural characterization and immunosuppressive activities of *Ligularia fischeri*, a plant mainly found in mainland China, secondary metabolites (Gobu *et al.*, 2017). DDD was isolated and its structure characterized but wasn't found to prohibit the growth of human B lymphoblastoid cells but rather it promoted cell proliferation (Gobu *et al.*, 2017). Similarly, in "*Two New Dolabrane Diterpenes from the Chinese Mangrove Ceriops taga,l*" we found dolabranes extracted from the Chinese mangrove *Ceriops tagal* with sub-structural similarity to the new metabolites NDA, DHD, and DA. Compounds were isolated mainly for the purposes of testing their anti-tumor activity.

Epoxydolabrene an established product of ZmCYP71Z16 (Mafu et al., 2018) was also present in high concentrations in the same tissues that had detectable levels of NDA-ME and DDD. This provides evidence that DDD and NDA are products of enzyme-mediated oxidation of dolabradiene, specifically Z16 mediated oxidation.

Through forward genetic mapping efforts we were able to map to a gene cluster containing ZmCYP71Z16 and ZmCYP71Z18, other cytochrome P450 monooxygenases and epoxide hydrolases (Fig 8) (Ding *et al*. 2020). Knowing that epoxydolabranol is a product of ZmCYP71Z16 dolabradiene oxidation, we conducted ratio mapping trials in an effort to support hypothesized enzymatic oxidations stemming from epoxydolabranol (Fig 8). Observing the increases in statistical significance from the mapping trait epoxydolabranol to the ratio of DA/epoxydolabranol (Fig 8A-F) we believe that a gene encoding an enzyme responsible for the further processing of novel dolabralexins found in this study exist on Chromosome 5 within a locus spanning 200 genes surrounding ZmCYP71Z16 and ZmCYP71Z18.

Additionally, we are leveraging the power of MR to lead us to the genes and corresponding enzymes that catalyze the enzymatic steps that produce the novel dolabralexins. Through MR analyses we have now greatly narrowed the list of candidate neighboring genes on chromosome 5, that could be further contributing to the dolabralexin pathway and will be performing gene synthesis on *ZmCYP89A6* (*Zm00001d014335*) and an *epoxide hydrolase* (*Zm00001d013934*) shown to have to use in *Agrobacterium*-mediated transient overexpression enzyme assays (Fig 9). Unfortunately, due to the COVID-19 situation, we were unable to continue our pursuit of additional metabolites, uncharacterized compounds mentioned in above in figure 1. B, that we suspect are additional members of the dolabralexin pathway.

Collectively, the assays and analyses in our study have allowed us to hypothesize as to the position of these new metabolites in the greater maize diterpenoid defense biosynthetic map. Future efforts in expressing gene mapping candidates in *E. coli and N. benthamiana* will aid in the complete elucidation of the enzymatic steps that catalyze the formation of the new discovered dolabralexins.

References

Ahuja, Ishita, Ralph Kissen, and Atle M. Bones. 2012. "Phytoalexins in Defense against Pathogens." *Trends in Plant Science*.

Christensen, Shawn A., James Sims, Martha M. Vaughan, Charles Hunter, Anna Block, Denis Willett, Hans T. Alborn, Alisa Huffaker, and Eric A. Schmelz. 2018. "Commercial Hybrids and Mutant Genotypes Reveal Complex Protective Roles for Inducible Terpenoid Defenses in Maize." *Journal of Experimental Botany*.

Degenhardt, Jörg, Tobias G. Köllner, and Jonathan Gershenzon. 2009. "Monoterpene and Sesquiterpene Synthases and the Origin of Terpene Skeletal Diversity in Plants." *Phytochemistry*.

Devore, Natasha M., and Emily E. Scott. 2012. "Structures of Cytochrome P450 17A1 with Prostate Cancer Drugs Abiraterone and TOK-001." *Nature*.

Ding, Yezhang, Alisa Huffaker, Tobias G. Köllner, Philipp Weckwerth, Christelle A. M. Robert, Joseph L. Spencer, Alexander E. Lipka, and Eric A. Schmelz. 2017. "Selinene Volatiles Are Essential Precursors for Maize Defense Promoting Fungal Pathogen Resistance." *Plant Physiology*.

Ding, Yezhang, Katherine M. Murphy, Elly Poretsky, Sibongile Mafu, Bing Yang, Si Nian Char, Shawn A. Christensen, Evan Saldivar, Mengxi Wu, Qiang Wang, Lexiang Ji, Robert J. Schmitz, Karl A. Kremling, Edward S. Buckler, Zhouxin Shen, Steven P. Briggs, Jörg Bohlmann, Andrew Sher, Gabriel Castro-Falcon, Chambers C. Hughes, Alisa Huffaker, Philipp Zerbe, and Eric A. Schmelz. 2019. "Multiple Genes Recruited from Hormone Pathways Partition Maize Diterpenoid Defences." *Nature Plants*.

Ding, Yezhang, Philipp R. Weckwerth, Elly Poretsky, Katherine M. Murphy, James Sims, Evan Saldivar, Shawn A. Christensen, Si Nian Char, Bing Yang, Anh-dao Tong, Zhouxin Shen, Karl A. Kremling, Edward S. Buckler, Tom Kono, David R. Nelson, Jörg Bohlmann, Matthew G. Bakker, Martha M. Vaughan, Ahmed S. Khalil, Mariam Betsiashvili, Steven P. Briggs, Philipp Zerbe, Eric A. Schmelz, and Alisa Huffaker. 2020. "Genetic Elucidation of Complex Biochemical Traits Mediating Maize Innate Immunity." *BioRxiv*.

Flint-Garcia, Sherry A., Anne Céline Thuillet, Jianming Yu, Gael Pressoir, Susan M. Romero, Sharon E. Mitchell, John Doebley, Stephen Kresovich, Major M. Goodman, and Edward S. Buckler. 2005. "Maize Association Population: A High-Resolution Platform for Quantitative Trait Locus Dissection." *Plant Journal*.

Gage, Joseph L., Michael R. White, Jode W. Edwards, Shawn Kaeppler, and Natalia de Leon. 2018. "Selection Signatures Underlying Dramatic Male Inflorescence Transformation during Modern Hybrid Maize Breeding." *Genetics*.

Gobu, Fekadu Roge, Jian Jun Chen, Jun Zeng, Wen Jun Wei, Wei Feng Wang, Chang Jun Lin, and Kun Gao. 2017. “Isolation, Structure Elucidition, and Immunosuppressive Activity of Diterpenoids from Ligularia Fischeri.” *Journal of Natural Products*.

Harborne, Jeffrey B. 1999. “Modern Fungicides and Antifungal Compounds II; Edited by H. Lyr, P.E. Russell, H.W. Dehne and H.D. Sisler, Intercept Publishers, Andover, England, 1999. 505 Pp. ISBN 1-898298-60-2. £85.” *Phytochemistry*.

Huffaker, Alisa, Nicole J. Dafoe, and Eric A. Schmelz. 2011. “ZmPep1, an Ortholog of Arabidopsis Elicitor Peptide 1, Regulates Maize Innate Immunity and Enhances Disease Resistance.” *Plant Physiology*.

Huffaker, Alisa, Fatma Kaplan, Martha M. Vaughan, Nicole J. Dafoe, Xinzhi Ni, James R. Rocca, Hans T. Alborn, Peter E. A. Teal, and Eric A. Schmelz. 2011. “Novel Acidic Sesquiterpenoids Constitute a Dominant Class of Pathogen-Induced Phytoalexins in Maize.” *Plant Physiology*.

Köllner, Tobias G., Claudia Lenk, Christiane Schnee, Sabrina Köpke, Peter Lindemann, Jonathan Gershenzon, and Jörg Degenhardt. 2013. “Localization of Sesquiterpene Formation and Emission in Maize Leaves after Herbivore Damage.” *BMC Plant Biology*.

Kremling, Karl A. G., Shu Yun Chen, Mei Hsiu Su, Nicholas K. Lepak, M. Cinta Romay, Kelly L. Swarts, Fei Lu, Anne Lorant, Peter J. Bradbury, and Edward S. Buckler. 2018. “Dysregulation of Expression Correlates with Rare-Allele Burden and Fitness Loss in Maize.” *Nature*.

Mafu, Sibongile, Yezhang Ding, Katherine M. Murphy, Omar Yaacoobi, J. Bennett Addison, Qiang Wang, Zhouxin Shen, Steven P. Briggs, Jörg Bohlmann, Gabriel Castro-Falcon, Chambers C. Hughes, Mariam Betsiashvili, Alisa Huffaker, Eric A. Schmelz, and Philipp Zerbe. 2018. “Discovery, Biosynthesis and Stress-Related Accumulation of Dolabradiene-Derived Defenses in Maize.” *Plant Physiology*.

Ni, Shu Jun, Jun Li, and Min Yi Li. 2018. “Two New Dolabrane Diterpenes from the Chinese Mangrove Ceriops Tagal.” *Chemistry and Biodiversity*.

Pascual Teresa, J., A. F. Barrero, A. San Feliciano, and M. Medarde. 1980. “Eudesmane Alcohols from Jasonia Glutinosa.” *Phytochemistry*.

Sadre, Radin, Peiyen Kuo, Jiaxing Chen, Yang Yang, Aparajita Banerjee, Christoph Benning, and Bjoern Hamberger. 2019. “Cytosolic Lipid Droplets as Engineered Organelles for Production and Accumulation of Terpenoid Biomaterials in Leaves.” *Nature Communications*.

Samayoa, Luis Fernando, Rosa Ana Malvar, Bode A. Olukolu, James B. Holland, and Ana Butrón. 2015. “Genome-Wide Association Study Reveals a Set of Genes Associated with Resistance to the Mediterranean Corn Borer (Sesamia Nonagrioides L.) in a Maize Diversity Panel.” *BMC Plant Biology*.

Schmelz, Eric A., Juergen Engelberth, James H. Tumlinson, Anna Block, and Hans T. Alborn. 2004. “The Use of Vapor Phase Extraction in Metabolic Profiling of Phytohormones and Other Metabolites.” *Plant Journal*.

Schmelz, Eric A., Alisa Huffaker, James W. Sims, Shawn A. Christensen, Xuan Lu, Kazunori Okada, and Reuben J. Peters. 2014. “Biosynthesis, Elicitation and Roles of Monocot Terpenoid Phytoalexins.” *Plant Journal*.

Schmelz, Eric A., Fatma Kaplan, Alisa Huffaker, Nicole J. Dafoe, Martha M. Vaughan, Xinzhi Ni, James R. Rocca, Hans T. Alborn, and Peter E. Teal. 2011. “Identity, Regulation, and Activity of Inducible Diterpenoid Phytoalexins in Maize.” *Proceedings of the National Academy of Sciences of the United States of America*.

Turlings, Ted C. J., J. W. A. Scheepmaker, L. E. M. Vet, J. H. Tumlinson, and W. J. Lewis. 1990. “How Contact Foraging Experiences Affect Preferences for Host-Related Odors in the Larval Parasitoid Cotesia Marginiventris (Cresson) (Hymenoptera: Braconidae).” *Journal of Chemical Ecology*.

Vaughan, Martha M., Shawn Christensen, Eric A. Schmelz, Alisa Huffaker, Heather J. Mcauslane, Hans T. Alborn, Maritza Romero, Leon Hartwell Allen, and Peter E. A. Teal. 2015. “Accumulation of Terpenoid Phytoalexins in Maize Roots Is Associated with Drought Tolerance.” *Plant Cell and Environment*.

Wisecaver, Jennifer H., Alexander T. Borowsky, Vered Tzin, Georg Jander, Daniel J. Kliebenstein, and Antonis Rokas. 2017. “A Global Coexpression Network Approach for Connecting Genes to Specialized Metabolic Pathways in Plants.” *Plant Cell*.